

# Assessing the Effectiveness of SO<sub>2</sub>, NO<sub>x</sub>, and NH<sub>3</sub> Emission Reductions in Mitigating Winter PM<sub>2.5</sub> in Taiwan Using CMAQ Model

Ping-Chieh Huang<sup>1</sup>, Hui-Ming Hung<sup>1\*</sup>, Hsin-Chih Lai<sup>2</sup>, and Charles C.-K. Chou<sup>3</sup>

5 <sup>1</sup>Department of Atmospheric Sciences, National Taiwan University, Taipei, 106319, Taiwan

<sup>2</sup>Department of ~~Green Energy and Environmental Resources–Occupational Safety and Health~~, Chang Jung Christian University, Tainan, 71101301, Taiwan

<sup>3</sup>Research Center of Environmental Changes, Academia Sinica, Taipei, 115201, Taiwan

Correspondence to: Hui-Ming Hung ([hmhung@ntu.edu.tw](mailto:hmhung@ntu.edu.tw))

10 **Abstract.** Taiwan experiences higher air pollution in winter when fine particulate matter (PM<sub>2.5</sub>) levels frequently surpass national standards. This study employs the Community Multiscale Air Quality model to assess the effectiveness of reducing ~~SO<sub>2</sub>NH<sub>3</sub>~~, NO<sub>x</sub>, and ~~NH<sub>3</sub>SO<sub>2</sub>~~-emissions on PM<sub>2.5</sub> secondary inorganic species (i.e., SO<sub>4</sub><sup>2-</sup>, NO<sub>3</sub><sup>-</sup>, and NH<sub>4</sub><sup>+</sup>). For sulfate, ~43.7% is derived from the chemical reactions of local SO<sub>2</sub> emission, emphasizing the substantial contribution of regional transported sulfate. In contrast, nitrate and ammonium are predominantly influenced by local NO<sub>x</sub> and NH<sub>3</sub> emissions

15 ~~predominantly influence nitrate and ammonium~~. Reducing SO<sub>2</sub> emissions decreases sulfate levels, which in turn affects thereby influencing–NH<sub>3</sub> partitioning and resultsing in ~~a decreased~~lower ammonium concentrations. Similarly, reducing NO<sub>x</sub> emissions lowers HNO<sub>3</sub>, impacting nitrate and ammonium concentrations due to changes in HNO<sub>3</sub> and NH<sub>3</sub> partitioning. A particularly significant finding is that reducing NH<sub>3</sub> emissions ~~reduction~~–decreases not only ammonium and nitrate and ammonium but also sulfate by altering cloud droplet pH and SO<sub>2</sub> oxidation processes. While the impact of SO<sub>2</sub> reduction's on

20 PM<sub>2.5</sub> ~~impact~~–is less than NO<sub>x</sub> and NH<sub>3</sub>, it emphasizes the complexity of regional sensitivities. Most of western Taiwan is NO<sub>x</sub>-sensitive, so reducing NO<sub>x</sub> emissions has a more substantial impact on lowering PM<sub>2.5</sub>. However, given the higher mass emissions of NO<sub>x</sub> than NH<sub>3</sub> in Taiwan, NH<sub>3</sub> has a more significant consequence in mitigating PM<sub>2.5</sub> per unit mass emission reduction. The cost-effectiveness analysis suggests that NH<sub>3</sub> reduction outperforms SO<sub>2</sub> and NO<sub>x</sub>. Nevertheless, the costs of emission reduction ~~cost estimates~~–vary due to differences in methodologyical differences–and regional emission sources.

25 Overall, this study considers both efficiency and costs, highlighting NH<sub>3</sub> emissions reduction as a promising strategy for PM<sub>2.5</sub> mitigation in the studied Taiwan's environment.

## 1 Introduction

30 Aerosol particles in the atmosphere have become a significant concern due to their adverse health effects (Maynard et al., 2002; Shiraiwa et al., 2017; Sugiyama et al., 2020) and their role in affecting global radiation budgets (Ramanathan et al., 2001; IPCC, 2021). Long-term exposure to air pollutants such as particulate matter (PM) and ozone (O<sub>3</sub>) has been linked to millions of premature deaths annually on a global scale (Vohra et al., 2022; WHO, 2021). These findings emphasize the critical need for a comprehensive understanding of air pollution and effective management strategies to protect public health and  
35 mitigate environmental consequences.

PM can enter the atmosphere through direct emissions ~~of primary aerosols~~, such as black carbon, sea salt, dust, and certain organic substances. ~~Alternatively, PM or it~~ can be formed via chemical reactions ~~involving of~~ gas-phase precursors, ~~creating~~ ~~(secondary aerosols)~~, such as sulfate (SO<sub>4</sub><sup>2-</sup>), nitrate (NO<sub>3</sub><sup>-</sup>), and ammonium (NH<sub>4</sub><sup>+</sup>) (Seinfeld et al., 2006). The composition of PM varies globally, with organic and inorganic components representing major categories. Inorganic aerosol components,  
40 including sulfate, nitrate, ammonium, and chloride, constitute 35-% to 77-% of PM<sub>1</sub> worldwide (Schroder et al., 2018). The significant proportion of secondary inorganic composition can influence the pH value of PM, further impacting the formation of secondary organic matter (Zhang et al., 2007).

Sulfate is formed through both ~~gas-gas~~-phase and aqueous oxidation of sulfur dioxide (SO<sub>2</sub>) emitted from sources like coal power plants and industrial processes, while nitrate is produced via the oxidation of nitrogen oxides (NO<sub>x</sub>), mainly emitted  
45 from traffic. Ammonium can be formed through the partitioning between ~~the~~ aqueous and gas phases of ammonia (NH<sub>3</sub>) emitted from agricultural and industry sources. The overall sulfate-nitrate-ammonium formation processes are illustrated in Fig. 1. In addition to the gas phase reaction with OH radicals, SO<sub>2</sub> can also be oxidized ~~by oxidants~~, such as hydrogen peroxide (H<sub>2</sub>O<sub>2</sub>) or ozone (O<sub>3</sub>) in the aqueous phase. Due to the low volatility and high dissociation constant of sulfuric acid, most sulfuric acid is in the condensed phase and dissociates in aqueous particles. Ammonia and nitric acid are semi-volatile, so their  
50 dissolution in particles is determined by their Henry's law constant and dissociation constants. The presence of acid for ammonia or base for nitric acid can promote individual dissolution (Seinfeld et al., 2006). The interaction of sulfate, nitrate, and ammonium is vital in determining the quantity of PM.

Human activities and natural sources are responsible for releasing the inorganic aerosol precursors, i.e., SO<sub>2</sub>, NO<sub>x</sub>, and NH<sub>3</sub>. Reducing these emissions might mitigate PM<sub>2.5</sub> levels, thus improving air quality. Numerous studies have investigated  
55 emission reduction strategies, with a focus on NH<sub>3</sub> reductions showing promise in decreasing PM<sub>2.5</sub> levels (Chen et al., 2019; Gu et al., 2021). Liu et al. (2019) used the WRF-chem model to investigate emission reduction strategies in China and found that reducing SO<sub>2</sub> and NO<sub>x</sub> emissions alone does not significantly reduce total PM<sub>2.5</sub> levels. However, including controls for NH<sub>3</sub> emissions can reduce PM<sub>2.5</sub> by approximately 11-17-%, but with the potential risk of exacerbating acid rain. Derwent et al. (2009) employed a photochemical trajectory model to simulate PM concentrations in the UK with 30-% reductions in NH<sub>3</sub>,  
60 SO<sub>2</sub>, NO<sub>x</sub>, VOC, and CO emissions. In an ammonium-limited environment (southern UK), NH<sub>3</sub> emissions reductions had the most significant impact on PM reduction, exhibiting a non-linear dynamic effect.

In Taiwan, secondary inorganic aerosol constitutes 30-53% of PM<sub>2.5</sub>, with sulfate, nitrate, and ammonium contributing significantly (16-32%, 2-24%, and 6-12%, respectively) (Chuang et al., 2021). PM<sub>2.5</sub> concentrations in Taiwan are usually higher in winter than in summer due to the ~~influence of~~ meteorological conditions and the planetary boundary layer height.

65 ~~This effect is e~~Especially pronounced on the leeward side of the prevailing northeast monsoon in winter (i.e., ~~the~~ western Taiwan), where the impact of PM<sub>2.5</sub> concentration accumulation is more significant (Hsieh et al., 2022; Hsu et al., 2016; Lai et al., 2020). Even though ~~the~~ PM<sub>2.5</sub> concentration has decreased over the past two decades (Cheng et al., 2019; Chuang et al., 2021), the current PM<sub>2.5</sub> reduction effort might not efficiently meet the standard set by the Taiwan Ministry of Environment (TW-MOENV): a 24-hour standard of 35 µg m<sup>-3</sup> and annual level of 15 µg m<sup>-3</sup>. ~~Due to~~Given the complex  
70 interactions among secondary inorganic components and their substantial contribution to total PM in Taiwan, further research is imperative.

To study air pollution in Taiwan, we employed the Community Multiscale Air Quality (CMAQ) model, ~~which is~~ recognized for its comprehensiveness in simulating atmospheric chemical processes. The CMAQ model incorporates various chemical processes, including photolysis, multiphase chemistry, aerosol microphysics, aqueous chemistry in clouds, and cloud  
75 formation on particles (Byun et al., 2006). It is widely used to assess air pollutants on a regional scale and helps understand changes and mechanisms of pollutants under different scenarios. This study focuses on investigating the formation of secondary inorganic species, specifically sulfate, nitrate, and ammonium, during winter in Taiwan. ~~With an~~By understanding ~~of~~ the contribution of each composition contribution from different processes and their interaction, the reduction efficiency and cost of each aerosol precursor (i.e., SO<sub>2</sub>, NO<sub>x</sub>, and NH<sub>3</sub>) in mitigating PM<sub>2.5</sub> are evaluated.

## 80 **2 Methodology**

### **2.1 CMAQ model**

The Community Multiscale Air Quality (CMAQ) model, ~~using with~~ the Weather Research and Forecasting (WRF) model for meteorological conditions, was applied to simulate the concentrations of various chemical species over Taiwan. The WRF model version 3.7.1 (Skamarock et al., 2008) was initialized using a cold start and simulated the period from 28<sup>th</sup>  
85 November 2018 to 31<sup>st</sup> December 2018, with analysis focusing on December only. Four nested domains, as shown in Fig. S1a, were created with horizontal resolutions of 81, 27, 9, and 3 km and a total of 45 vertical layers. The outer domain covers most of East Asia and the western Pacific, while the inner domain was dedicated to Taiwan.

The CMAQ model version 5.2.1 (Byun et al., 2006; Wyat Appel et al., 2018) was set up using the same horizontal grid structure as WRF, but with 15 vertical layers as seven layers under 1500 m and the top layer ~17 km above the ground. The  
90 inner domain of CMAQ consists of 135 × 90 grid cells. The chemical mechanism used in the simulations was Carbon Bond Mechanism version 6 and aerosol module version 6 with aqueous chemistry (cb6r3\_ae6\_aq). Emission data for Taiwan were from the Taiwan Emission Data System (TEDS9.0) based on the 2013 data. TEDS9.0 provides comprehensive information

on various sources of pollutants in Taiwan, including industrial processes, transportation, energy production, and residential activities. Hourly model output data enables-allowed for detailed temporal analysis. Additional details on the model configuration, including physical and chemical mechanisms, are summarized in Tables S1 and S2.

## 2.2 Observation data in Taiwan

The simulated data of the control run were compared with observations from ground-based monitoring stations to validate the model outputs. Hourly meteorological parameters (air temperature, relative humidity, and wind field) and pollutants (CO, O<sub>3</sub>, and PM<sub>2.5</sub>) data were collected from TW-MOENV air quality monitoring stations. Four stations along the western coast of Taiwan (Fig. S1b), -including Tamsui (25.16° N, 121.45° E), Shalu (24.23° N, 120.57° E), Taixi (23.72° N, 102.20° E), and Qianzhen (22.61° N, 120.31° E) stations, were selected for comparisons of wind fields and PM<sub>2.5</sub> concentrations-comparisons. Additionally, intensive observation data using filter sampling were obtained from Shalu (24.24° N, 120.57° E), Chung Shan Medical University (24.12° N, 120.65° E, CSMU), Zhushan (23.76° N, 120.68° E), and Xitou (23.67° N, 120.80° E) in central Taiwan from 1<sup>st</sup> December to 21<sup>st</sup> December 2018. These data provided further insideinsights into PM<sub>2.5</sub> and its components. Sampling occurs from 9:00 to 18:00 for daytime samples and from 21:00 to 6:00 (next day) for nighttime samples. Inorganic ions were analyzed using ion chromatography (IC). More details of-on the analytical methodology can be found in Chen et al. (2021) and Lee et al. (2019).

## 2.3 CMAQ experimental design

To evaluate the contribution of the sulfate pathway and the impact of aerosol precursor emission reduction at-on mitigating PM<sub>2.5</sub> levels, we designed the following two series of experiments.

### 2.3.1 Sulfate contributionsources

The local sulfate in PM<sub>2.5</sub> (PM-sulfate) can be contributed from transport and local gas phase and aqueous phase chemical reactions. To assess the contribution of each source to the local PM-sulfate within the inner domain, adjustments were made to the chemical reaction module within the CMAQ chemistry-transport model (CCTM). This analysis involved two simulations: "NoAqChem run" and "NoChem run". In NoAqChem run, sulfur aqueous phase oxidation reactions, including S(IV) oxidation by O<sub>3</sub>, H<sub>2</sub>O<sub>2</sub>, organic peroxides, and metal ion catalysis (Jacobson, 1997), were turned off. In NoChem run, all chemical reactions in CMAQ were disabled. By comparing the PM-sulfate of these simulations with the control run, the contribution fractions of gas phase ( $F_{gas}$ ) and aqueous phase ( $F_{aq}$ ) reactions to local PM-sulfate were evaluated using the following equations:

$$F_{gas} = \frac{NoAqChem\ run - NoChem\ run}{Control\ run} \times 100\% \quad (1)$$

$$F_{aq} = \frac{Control\ run - NoAqChem\ run}{Control\ run} \times 100\% . \quad (2)$$

### 2.3.2 Emission reduction efficiency

Our study assessed variations in PM<sub>2.5</sub> and major inorganic composition concentrations resulting from emissions reductions. Specifically, we focused on modifying SO<sub>2</sub>, NO<sub>x</sub>, and NH<sub>3</sub> emissions proportionally, as these are key aerosol precursors forming sulfate, nitrate, and ammonium in aerosols. The emissions of SO<sub>2</sub>, NO<sub>x</sub>, and NH<sub>3</sub> are 1.18×10<sup>6</sup>, 4.61×10<sup>6</sup>, and 1.77×10<sup>6</sup> tons yr<sup>-1</sup>, respectively, based on the applied emission inventory. Emissions were reduced individually at intervals of 0.2 (i.e., 0.8x, 0.6x, 0.4x, and 0.2x of the control-run emissions) in the inner domain, labeled as the "ER1 runs". Additionally, the effects of potential earlier emission quantities were explored by increasing emissions at 0.5 intervals (i.e., at 1.5x and 2.0x of the control-run emissions), referred to as "EI runs". Considering the interplay between nitrate and ammonium due to acid-base balance, we conducted "ER2 runs", reducing both NO<sub>x</sub> and NH<sub>3</sub> emissions at 0.2 intervals. Notably, "ER2 runs" covers the first half of December (from 1<sup>st</sup> ~~December~~ to 14<sup>th</sup> December) to save computing resources, while other simulations encompassed the entire month. Table 1 provides a summary of all simulation settings.

The variation of aerosol composition and PM quantity based on emission adjustment is evaluated to assess the sensitivity and effectiveness of emission reduction. Following Takahama et al. (2004), a dimensionless sensitivity coefficient ( $S_{X,Y}$ ) was introduced to evaluate the potential impacts of  $X$  emission reduction on  $Y$  (nitrate or PM<sub>2.5</sub>) as follows:

$$S_{X,Y} = \frac{E_X}{Y} \frac{dY}{dE_X} = \frac{d\log(Y)}{d\log(E_X)} \approx \frac{\Delta\log(Y)}{\Delta\log(E_X)}, \quad (3)$$

where  $E_X$  represents the specific emission of SO<sub>2</sub>, NO<sub>x</sub>, and NH<sub>3</sub>.  $\Delta(\text{var})$  is the difference between  $\text{var}_i$  and  $\text{var}_{i-1}$ , two adjacent points. For  $Y = \text{nitrate}$ , the sensitivity is sensitive to NO<sub>x</sub> and-or NH<sub>3</sub>. A higher response among the given emission reductions indicated the properties of the environment, such as NO<sub>x</sub>-sensitive or NH<sub>3</sub>-sensitive (Petetin et al., 2016). This framework can also assess the potential sensitivity of emission reductions on PM<sub>2.5</sub> concentration (i.e.,  $Y = \text{PM}_{2.5}$ ) for each emission. A higher sensitivity under  $E_X$  reduction indicates that more significant PM<sub>2.5</sub> mitigation can be achieved by controlling this emission.

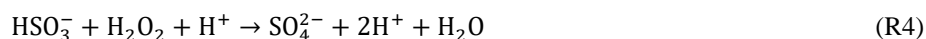
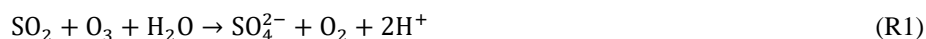
### 2.4 Box model

A simplified box model, constructed using Python, was developed to study the influence of NH<sub>3</sub> emissions on sulfate formation, specifically-focusing specifically on the chemical reactions occurring in the aqueous phase. These reactions, including-include dissolution, oxidation, and dissociation processes (Reactions 5-8 in Table 2). The model aimed to assess the impact of ammonia emission reduction on sulfate formation, focusing-on~~considering~~ only chemical processes only-with fixed meteorological conditions and no physical transport. The box model conditions were adapted from a grid point of CMAQ within the planetary boundary layer that exhibiteding sufficient liquid water content (LWC). To retrieve the initial concentrations of reactants, the maximum attention-concentrations of oxidants (O<sub>3</sub> and H<sub>2</sub>O<sub>2</sub>) along the ammonia reduction profile was-were applied, with an equal amount of sulfate back-reverted to SO<sub>2</sub>. The input parameters from CMAQ, including including air temperature (T), liquid water content, and concentrations of SO<sub>2</sub>, carbon dioxide (CO<sub>2</sub>), total nitric acid (HNO<sub>3</sub>), total NH<sub>3</sub>, H<sub>2</sub>O<sub>2</sub>, O<sub>3</sub>, S(IV), iron (Fe(III)), and manganese (Mn(II)), were from CMAQ and summarized. A summary of the

~~initial conditions employed in this study is provided~~ in Table S3. Similar to the aqueous phase reactions ~~of-in~~ CMAQ, the dissolution of chemical components in water follows the equilibrium between the gas ~~and-to-dissolved~~ aqueous phases controlled by Henry's constants. The initial pH value was calculated based on the acid-base balance and charge balance ~~Eq. (4)~~ of the system, ensuring consideration ~~among-of~~ different chemical species and their influence on the overall pH ~~in the following equation:-~~

$$[H^+] = [OH^-] + [HCO_3^-] + 2[CO_3^{2-}] + [HSO_3^-] + 2[SO_3^{2-}] + 2[SO_4^{2-}] + [NO_3^-] - [NH_4^+] \quad (4)$$

At each time step, the model calculated concentration changes ~~following-based on~~ the oxidation reactions, and the pH value was recalculated at the new equilibrium state. The oxidation reactions considered in the box model are as follows (Seinfeld et al., 2006):



~~with-~~The rate constants ~~for these reactions are~~ summarized in Table S4.

Two sets of experiments were conducted to compare the results with those ~~of-from~~ the CMAQ ~~simulations~~. These ~~experiments/simulations~~ were conducted by gradually reducing NH<sub>3</sub> emissions ~~at-in~~ 0.1x intervals. The first set exclusively considered the oxidation reactions of S(IV) by O<sub>3</sub> and H<sub>2</sub>O<sub>2</sub> (i.e., R2+R3), while the second set ~~incorporated-included~~ additional oxidation reactions of S(IV) by O<sub>2</sub>, ~~with-cataly~~ sized ~~of-by~~ iron and manganese (i.e., R2+R3+R4). The timestep of these experiments was ~~set to~~ 0.05 seconds, and results from a 10-minute run were analyzed. ~~as-~~The oxidation reaction levels ranged from 65.1 to 99.9-% ~~compared-to~~ of the 1-hour reaction, depending on the emission reduction ratio. The box model results reflect the impact of ammonia emission on sulfate formation under specific conditions. However, the composition of a grid box in CMAQ is influenced by chemical processes and transport. ~~soation-~~ The overall results between the box model and CMAQ may not match precisely.

## 2.5 Mitigation efficiency and cost estimation

To evaluate the effectiveness of PM<sub>2.5</sub> reduction, we employed an exponential function to fit PM<sub>2.5</sub> concentration as a function of emission adjustment ratios ranging from 0.2x to 2.0x of control-run emissions. The derivative of PM<sub>2.5</sub> ~~concentration~~ or the quantity of a specific component (Y) ~~with respect to concerning~~ emissions was applied to assess the emission reduction efficiency of X (~~where~~ X can be SO<sub>2</sub>, NO<sub>x</sub>, or NH<sub>3</sub>), denoted as follows:

$$Y \text{ reduction efficiency} = \frac{dY}{dE_X} [\mu\text{g m}^{-3} \cdot \text{ton}^{-1}\text{yr}] \quad (5)$$

The cost of PM<sub>2.5</sub> reduction is evaluated by dividing the marginal abatement cost (MAC) by PM<sub>2.5</sub> reduction efficiency (obtained from Eq. (5) with  $\bar{Y}$  as PM<sub>2.5</sub>) as follows:

$$PM_{2.5} \text{ reduction cost} = \frac{MAC}{PM_{2.5} \text{ reduction efficiency}} [\text{USD yr}^{-1} \cdot \mu\text{g}^{-1}\text{m}^3]. \quad (6)$$

The applied MAC values are 421-1630 USD ton<sup>-1</sup>, 8152-9570 USD ton<sup>-1</sup>, and 1318-1400 USD ton<sup>-1</sup> for SO<sub>2</sub>, NO<sub>x</sub>, and NH<sub>3</sub>, respectively, based on the studies of Gu et al. (2021) and Kaminski (2003).

## 3 Results and Discussion

### 3.1 Model performance

#### 3.1.1 Meteorology

The comparison between WRF model results and TW-MOENV observations is presented in Tables 3 and S5, providing a comprehensive overview of monthly mean values, correlation coefficients (r), mean bias errors, mean absolute error, mean fractional bias, and mean fractional errors. Notably, the correlation coefficients for air temperature consistently exceed 0.8 across all four stations, showcasing a robust agreement. For relative humidity, the correlation coefficients range from 0.71 to 0.86, indicating a good alignment between observation and model results. For wind speed, the correlation coefficients range from 0.42 to 0.85 at these stations. The mean bias error at Shalu and Qianzhen meets the criteria suggested by Hu et al. (2016), while the mean absolute error at Tamsui, Shalu, and Qianzhen also meets the criteria. At Taixi, the model tends to ~~is mostly underestimate~~ be underestimated, resulting ~~in the model to have~~ a higher mean absolute error. Overall, these findings demonstrate ~~a satisfactory~~ model ~~performance of the model.~~

Wind fields play a critical role in the dispersion of air pollutants, affecting their transport and spatial distribution, not only for wind speed but for wind direction. Fig. S2 illustrates that the model reasonably captures the prevailing winter wind patterns, characterized by predominant winds blowing from the northeast. Although discrepancies in wind speed exist, with slight underestimations in Taixi and overestimations in Tamsui, Shalu, and Qianzhen, the overall trend of strong and weak winds is consistent between the model and observations.

#### 3.1.2 Air pollutants

Table S5 also provides statistical results for pollutants. The correlation coefficients between observation and model range from 0.46 to 0.62 for CO and from 0.58 to 0.84 for O<sub>3</sub>. The mean bias errors are higher for both CO and O<sub>3</sub>, likely due to a significant underestimation of CO and an overestimation of O<sub>3</sub> in the model results. For PM<sub>2.5</sub>, the model exhibits good agreement with observations, capturing similar concentration patterns. Specifically, lower PM<sub>2.5</sub> concentrations were observed under more vital northeasterly wind conditions, while weaker northeasterly winds or winds from other directions corresponded to higher

pollutant concentrations. The correlation coefficients for PM<sub>2.5</sub> concentration range from 0.42 to 0.71, and the mean fractional bias and mean fractional error for PM<sub>2.5</sub> are within the acceptable criteria (Table 3), affirming the model's reliability (Fig. S2). For the spatial distribution of PM<sub>2.5</sub>, ~~areas with~~ high pollution levels are primarily concentrated in western regions, corresponding to densely populated areas (Fig. S3a). The PM<sub>2.5</sub> concentration gradually increases from north to south, mainly over flat land areas. To assess ~~the~~ regional distribution, we used regional-area average concentration and partitioning of PM<sub>2.5</sub>, based on TW-MOENV's pollutant zone classification (Fig. S3b), focusing on areas with altitudes-elevation less than 200 m above sea level (a.s.l.) to avoid complexities in terrain. The partitioning of PM<sub>2.5</sub> is similar across regions, with secondary inorganic components constituting more than half of PM<sub>2.5</sub>.

This study focuses on central Taiwan, specifically the marked red area on the map (Fig. S3b). In the control run, the surface layer mean PM<sub>2.5</sub> in central Taiwan has-shows a similar pattern to nitrate and ammonium, while sulfate has some slight differences (blue line in Fig. S4). The correlation coefficient between PM<sub>2.5</sub> and sulfate, nitrate, and ammonium are 0.65, 0.96, and 0.95, respectively. Given the high correlation between nitrate and ammonium ( $r = 0.98$ ) and the significant contribution of nitrate to PM<sub>2.5</sub> concentrations in Taiwan, nitrate emerges as a major contributor to PM<sub>2.5</sub>. ~~In-Additionally~~, we ~~notice~~ observe that ~~the-pollutant~~ concentrations ~~of-pollutants is~~are related to the wind strength ~~of-the-wind field~~. Combined with Shalu's wind field time series ~~diagram~~, representing the environmental wind in central Taiwan, nitrate, ammonium, PM<sub>2.5</sub>, and wind speed have-show a certain negative correlation, while sulfate is less relevant-affected. This suggests that gaseous HNO<sub>3</sub> and NH<sub>3</sub> accumulate locally during weak wind conditions, facilitating the transformation of nitrate and ammonium into aerosol particles.

The correlation coefficients of PM<sub>2.5</sub> between observation and model at Shalu and CSMU are 0.76 and 0.65, respectively, ~~and-demonstrating the~~ consistency of model results for concentration and change trend ~~in-at~~ these two stations ~~can-also-be-seen in-~~(Fig. S5). However, the correlation between observational ~~data~~ and model ~~data~~ at Zhushan and Xitou is poor, which may be likely due to the influence of the complex topography ~~of-at~~ these two places. Further analysis in Fig. S6 presents the trends and correlation coefficients for PM-sulfate, PM-nitrate, and PM-ammonium across the four stations. The data reveals a slight underestimation trend for PM-sulfate, particularly at Shalu and Zhushan. The simulation for PM-ammonium appears reasonably accurate, whereas PM-nitrate shows a tendency for overestimation. The simulated proportions of PM-sulfate, PM-nitrate, and PM-ammonium formation by CMAQ are 9.1-11.4-%, 18.7-34.9-%, and 9-13.7-%, respectively. In contrast, the observation data indicates that proportions of PM-sulfate, PM-nitrate, and PM-ammonium formation are 13.9-19.6-%, 16.6-22.8-%, and 7.6-10.7-%, respectively (Fig. 2). Considering the spatial heterogeneity of PM<sub>2.5</sub>, our analysis mainly discusses-focuses on examining the composition of PM<sub>2.5</sub> rather than emphasizing the differences between the model outputs and observational data. Overall, in central Taiwan's average model data and single-point observation data, secondary inorganic aerosols account for approximately half of the concentration of PM<sub>2.5</sub>, ~~of-which-with~~ nitrate ~~is-being~~ the highest contributor.



### 3.2 Sulfate formation pathways ~~on PM<sub>2.5</sub>~~

With the analysis of NoAqChem and NoChem runs, the mean contributions ~~of to~~ sulfate in central Taiwan are as follows: 13.2 % from gas reactions, 30.5-% from aqueous reactions, and 56.3-% from other processes. ~~These other processes include~~ the ~~transportation~~ from ~~the~~ domain boundary, locally emitted primary sulfate (constituting less than 5-% of SO<sub>2</sub> emissions), and alterations of deposition. The analysis for other areas is summarized in Table S6, with all chemical processes ~~accounting for having a portion~~ less than 50-% ~~of the contributions~~. The major aqueous reactions occur in the cloud, typically with higher cloud water content (QC). ~~By Comparing~~ the time series of average cloud water content in the boundary layer (Fig. S67a) ~~shows, it becomes evident~~ that high QC corresponds to dominant aqueous chemical processes in sulfate formation. The correlation coefficient between QC and the sulfate difference (control run - NoAqChem run) is 0.65, ~~(indicating the significant contribution of aqueous phase chemical processes)~~. ~~Additional More details regarding the~~ correlation coefficients of PM ~~concentration composition~~ and meteorological parameters are ~~available detailed~~ in Table 4. Nitrate and ammonium concentrations exhibit a stronger relationship with the wind field, while sulfate concentration is more influenced by the occurrence of aqueous phase chemistry, specifically the amount of cloud water content in the atmosphere. In addition, the contribution of aqueous chemical processes is ~~also~~ highly correlated with sulfate concentration in the control run, particularly during periods of elevated sulfate levels. However, ~~the impact of these sulfate changes in sulfate have an insignificant impact on nitrate, ammonium, and PM<sub>2.5</sub> is insignificant~~ (Fig. S4). Given that nitrate ~~constitutes comprises~~ a significant proportion of PM<sub>2.5</sub> during the winter in Taiwan, our results suggest that the overall trend of total PM<sub>2.5</sub> ~~aligns are~~ more closely with the wind ~~field patterns (ventilation efficiency with nitrate formation) rather than solely the contributions from sulfate formed via aqueous phase chemistry~~.

### 3.3 Emission ~~affecting effects PM<sub>2.5</sub> on the surface layer PM<sub>2.5</sub>~~

#### 3.3.1 Trends ~~of in~~ concentration

The impact of emission adjustments on PM<sub>2.5</sub> and its components in central Taiwan is shown in Fig. 3. PM<sub>2.5</sub> and secondary inorganic components show a decreasing trend as the emission ratio is reduced. ~~At When the~~ emission ratio ~~larger than exceeds~~ 1, ~~the variation in~~ PM<sub>2.5</sub> ~~variation is~~ relatively flat compared ~~to when the with~~ emission ratio ~~is below less than~~ 1. This indicates a higher PM<sub>2.5</sub> mitigation efficiency for future emission reduction. Reductions ~~of in~~ SO<sub>2</sub> primarily decrease sulfate and ammonium, while NO<sub>x</sub> reductions affect nitrate and ammonium. ~~However Conversely,~~ NH<sub>3</sub> reductions decrease ammonium, nitrate, and sulfate ~~levels~~. Since SO<sub>2</sub> is a ~~sulfate~~-precursor ~~to sulfate~~, reducing SO<sub>2</sub> decreases sulfate formation, consequently modifying the ammonia partition and decreasing ammonium ~~concentration~~ (Tsimpidi et al., 2007). The negligible impact on nitrate can be attributed to nitric acid partition processes, ~~which are~~ affected by particle acidity and available aerosol water content. With decreased ammonium and sulfate, the available water content in aerosols decreases, adversely influencing nitric acid partitioning to aerosols. Although reduced sulfate formation promotes more nitric acid partitioning, thermodynamic calculations indicate ~~that the reduced water content, causing leads to a the observed~~ decline in dissolved nitrate.

For NO<sub>x</sub>, reducing NO<sub>x</sub> emissions results in a lower HNO<sub>3</sub> formation, leading to a significant reduction in PM-nitrate. The ~~reduced-decreased~~ acidity contribution from nitric acid alters the partition of ammonia, ~~resulting-incausing~~ a decrease in ammonium. In contrast, the slight increase ~~in~~ sulfate formation ~~observed~~ may be attributed to enhanced chemical processes under lower NO<sub>x</sub> conditions. Reducing NO<sub>x</sub> emissions consumes less OH, a major pathway for HNO<sub>3</sub> formation during the daytime, as depicted in Reaction 2 of Table 2. The increased availability of OH can enhance the oxidation of SO<sub>2</sub> to form sulfuric acid through Reaction 1 in Table 2 (Derwent et al., 2009).

Regarding NH<sub>3</sub> emission reduction, NH<sub>3</sub> primarily acts as a base, influencing the dissolution of volatile acids such as HNO<sub>3</sub>. ~~With-Since~~ nitrate ~~having-has~~ a higher molecular weight than ammonium, the most significant decrease in mass concentration is observed for nitrate. Sulfuric acid, with negligible volatility, predominantly ~~participates-remains~~ in the aerosol phase. The observed decrease in sulfate is likely ~~attributed-due~~ to altered chemical processes influenced by NH<sub>3</sub>, particularly the aqueous reactions. ~~Further-exploration-of-~~The interplay between NH<sub>3</sub> reduction and sulfate ~~formation~~ will be discussed in more detail in Section 3.4.

With the ~~reduction-insignificant~~ PM<sub>2.5</sub> ~~mitigation~~ attributed to NO<sub>x</sub> or NH<sub>3</sub>, the response of PM<sub>2.5</sub>, sulfate, ammonium, and nitrate at various levels of ~~reduction-in-both~~ NO<sub>x</sub> and NH<sub>3</sub> ~~reduction~~ are shown in Fig. S7S8. For a given reduction in NO<sub>x</sub> (or NH<sub>3</sub>), the trends of interested species as a function of NH<sub>3</sub> (or NO<sub>x</sub>) ~~is-are~~ consistent ~~with-similar-to~~ the case discussed in Fig. 3. When both emissions are reduced, the contour of PM<sub>2.5</sub> is concave upward, indicating that the ~~mitigation-concentration~~ ~~efficiency~~ is ~~lower-less~~ than the linear combination of individual influence on PM<sub>2.5</sub>. A similar pattern ~~happened-is-observed~~ ~~for~~ PM-nitrate and PM-ammonium, while PM-sulfate exhibits ~~a~~ relatively smaller and different changes ~~s-trend~~. These results suggest that ~~the-changes~~ in PM<sub>2.5</sub> concentration ~~is-are~~ mainly dominated by nitrate and ammonium, with sulfate having a minor effect ~~on the studied environment~~. The deviation from the linear combination of individual contributions might be due to the variation in the partitioning between gas and aerosol phases under different acidity ~~levels~~. For example, NH<sub>3</sub> might have an increased portion in the gas phase as NO<sub>x</sub> is decreased, while HNO<sub>3</sub> would have a higher portion in the gas phase as NH<sub>3</sub> is reduced. ~~The-f~~Further reduction of the other species would ~~then~~ reflect ~~a higher portion reduction of gas phase concentration~~ ~~and~~ a lower portion reduction of PM-related species. Therefore, it can be inferred that as emission reductions reaches a certain level, the available nitric acid or ammonia is continuously reduced to ~~very-low~~ ~~enough~~ levels, potentially leading to a decline in the efficiency of PM<sub>2.5</sub> emission reduction (Veratti et al., 2023).

### 3.3.2 Sensitivity analysis

The sensitivity evaluation for different emission species on PM-nitrate and PM<sub>2.5</sub> is shown in Fig. 4. In the case of PM-nitrate sensitivity,  $S_{NO_x,NO_3}$  increases as the emission ratio decreases and reaches a maximum value of 0.83 at ~~the-an~~ emission ratio around 0.4-0.8 (using control run as a base value). Subsequently,  $S_{NO_x,NO_3}$  gradually decreases as the emission ratio ~~continues~~ ~~to~~ ~~decreases~~. This transition ~~in-the-~~ $S_{NO_x,NO_3}$  is likely due to the available quantity of NO<sub>2</sub> for HNO<sub>3</sub> formation via ~~the~~ NO<sub>2</sub> + OH reaction. In addition to being produced by chemical reactions, HNO<sub>3</sub> concentration is also affected by the transported

HNO<sub>3</sub> from the domain boundaries. While the transported HNO<sub>3</sub> concentration is relatively low compared to HNO<sub>3</sub> produced by local NO<sub>x</sub> emissions in Taiwan, its proportion gradually increases as NO<sub>x</sub> emissions decrease. When the HNO<sub>3</sub> concentration produced by the local chemical reaction is comparable to the transported concentration, the sensitivity coefficient decreases. (Detailed mathematical verification is provided in Section S1).

310 In contrast,  $S_{NH_3,NO_3}$  increases monotonically as the emission ratio decreases within the studied range, showing the significant influence of local NH<sub>3</sub> emission on PM-nitrate quantity. In the studied environmental context, a higher  $S_{NO_x,NO_3}$  than  $S_{NH_3,NO_3}$  indicates that PM-nitrate is more sensitive to NO<sub>x</sub> emissions in central Taiwan. The sensitivity on PM-nitrate in spatial distribution (Fig. S8a-S9a) shows that the major cities in western Taiwan and the southwest offshore are in a NO<sub>x</sub>-sensitive environment, while only the eastern region is biased toward NH<sub>3</sub>-sensitive, likely due to relatively low NH<sub>3</sub> and NO<sub>x</sub> emissions.

315 As to the sensitivity on PM<sub>2.5</sub>, the trend-influence of NO<sub>x</sub> sensitivity-emissions reduction ( $S_{NO_x,PM_{2.5}}$ ) is similar to  $S_{NO_x,NO_3}$ , as a reduction in NO<sub>x</sub> emissions primarily leads to a decrease in nitrate, exerting a dominant influence on PM<sub>2.5</sub> concentration.  $S_{NH_3,PM_{2.5}}$  and  $S_{SO_2,PM_{2.5}}$  are relatively stable.  $S_{SO_2,PM_{2.5}}$  gradually declines as the emission ratio decreases, while  $S_{NH_3,PM_{2.5}}$  first shows an-increases first as the emission ratio > 0.8 and then slightly decreases slightly. For the overall emission ratio range studied,  $S_{NH_3,PM_{2.5}}$  is around 0.19±0.01 while  $S_{NO_x,NO_3}$  has a wider range from 0.05 to 0.24, and  $S_{SO_2,PM_{2.5}}$  is 0.05±0.01. Under the studied condition (at the emission ratio of 0.9 in Fig. 4b),  $S_{SO_2,PM_{2.5}}$  (~ 0.05) is the lowest, while  $S_{NO_x,PM_{2.5}}$  (~ 0.23) and  $S_{NH_3,PM_{2.5}}$  (~ 0.2) are relatively higher, indicating that reducing NO<sub>x</sub> or NH<sub>3</sub> emissions results in a more significant reduction in PM<sub>2.5</sub> compared to reducing SO<sub>2</sub> emissions.

325 The sensitivity on PM<sub>2.5</sub> in spatial distribution (Fig. S89b) and the statistical data for each area (Table S7) show that  $S_{NO_x,PM_{2.5}}$  is greater than  $S_{NH_3,PM_{2.5}}$  in each air pollution zone, emphasizing the importance of NO<sub>x</sub> reduction in improving PM<sub>2.5</sub>. However, in the northern, Chu-Miao, and central areas,  $S_{NO_x,PM_{2.5}}$  and  $S_{NH_3,PM_{2.5}}$  are relatively close-similar. These areas have some white shading, indicating neutrality, and suggest that the reduction of NO<sub>x</sub> and NH<sub>3</sub> emissions is equally important.

### 3.4 Emission affecting impacts-effects on sulfate formation

#### 3.4.1 Composite results in cloud

330 The observed decrease in sulfate levels with a lower NH<sub>3</sub> emission ratio (Figs. 3c and S7b-S8b) is likely attributed to the modified cloud pH, affecting aqueous phase sulfate production (Redington et al., 2009), as NH<sub>3</sub> emissions do not directly impact the gas-phase chemistry of SO<sub>2</sub>. To preserve-capture the critical features, the-composite results from grid points containing clouds with significant SO<sub>2</sub> (i.e., a cloud water content ≥ 0.1 g kg<sup>-1</sup> and SO<sub>2</sub> concentration ≥ 1 ppbv when NH<sub>3</sub> is at 0.2x) are depicted in Figs. S9-S10 and S110 for land and sea regions, respectively. This categorization takes into account variations in pollutant levels between these two regions, and-the statistical summaries, including mean, 25th, and 75th percentile of cloud pH value and gaseous components, are provided in Table 4. While the mean pH values are higher over land

than at sea, ~~the majority of most~~ grid ~~pointss~~ have a pH of 5, slightly below the average. Notably, grid points with lower pH values are predominantly characterized by NH<sub>3</sub> deficiency, especially at sea, where the concentrations of NH<sub>3</sub> are lower than ~~these~~ on land.

340 The changes in chemical substances for both land and sea show consistent trends with emission reduction, featuring with higher concentrations of sulfate at sea compared to on land. The pattern of sulfate formation in clouds ([Figs. S10b and S11b](#)) is consistent with the average concentrations in the surface layer (Fig. [S7bS8b](#)), increasing with NO<sub>x</sub> emission reduction and decreasing with NH<sub>3</sub> emission reduction. Conversely, the concentration change of SO<sub>2</sub> ~~opposed-is opposite~~ that of sulfate due to the conservation of sulfur. A decrease in sulfate concentration implies that more sulfur remains as SO<sub>2</sub> in the atmosphere, indicating weaker oxidation reactions. Furthermore, the reduction of NH<sub>3</sub> also impacts primary oxidants involved in sulfur oxidation, namely H<sub>2</sub>O<sub>2</sub> and O<sub>3</sub>. Intriguingly, the changes in H<sub>2</sub>O<sub>2</sub> and O<sub>3</sub> exhibit opposite trends in response to NH<sub>3</sub> emission reduction ([Figs. S10c and S10d](#)), suggesting a potential influence on their oxidation rates.

The aqueous oxidation pathways of SO<sub>2</sub> are strongly pH-dependent. The oxidation rate by H<sub>2</sub>O<sub>2</sub> increases with pH < 3 and remains fairly constant at pH > 3 (Seinfeld et al., 2006). The other three reactions (O<sub>3</sub> and O<sub>2</sub> catalysis by Fe(III) and Mn(II)) are pH-dependent and increase with pH. Overall, H<sub>2</sub>O<sub>2</sub> oxidation is usually a major process. However, with an increase in pH, the oxidation rates of O<sub>3</sub> and O<sub>2</sub> catalysis via Fe(III) or Mn(II) might surpass that of H<sub>2</sub>O<sub>2</sub> if high enough Fe(III) or Mn(II) relative to H<sub>2</sub>O<sub>2</sub> presents.

### 3.4.2 Case analysis of a single grid point

The condition of a grid point along the coast of Taichung (24.203° N, 120.5053° E, the second layer, ~ 68.5 m a.s.l.) at 8:00 am local time on 3<sup>rd</sup> December 2018 from CMAQ was selected [for further analysis](#). This grid point fulfills our desired criteria, featuring a cloud water content of 0.376 g kg<sup>-1</sup> and an SO<sub>2</sub> concentration of 7.13 ppbv. Figure 5 shows the concentrations of SO<sub>2</sub>, H<sub>2</sub>O<sub>2</sub>, O<sub>3</sub>, and acidity (i.e., [H<sup>+</sup>]) in cloud water, calculated from CMAQ output data) at this grid point ~~from CMAQ~~ as a function of NH<sub>3</sub> and NO<sub>x</sub> emission ratios. With NH<sub>3</sub> emission reduction, SO<sub>2</sub> concentration increases significantly, especially when the NH<sub>3</sub> emission ratio ~~is falls~~ below 0.4, while the concentration decreases slightly as ~~the~~ NO<sub>x</sub> emission decreases. The pattern for acidity ~~mirrorsis similar to~~ that of SO<sub>2</sub>, showing an increase as NH<sub>3</sub> emissions decrease and a smooth decrease as NO<sub>x</sub> emissions decrease. This suggests a ~~possible~~ strong correlation between SO<sub>2</sub> and acidity, [likely due to a common influencing factor, NH<sub>3</sub>](#). As NO<sub>x</sub> emission decreases, the concentrations of both H<sub>2</sub>O<sub>2</sub> and O<sub>3</sub> increase due to changes in gaseous chemical reactions that reduce the consumption of OH and O<sub>3</sub>. When NH<sub>3</sub> emissions decrease, O<sub>3</sub> increases and H<sub>2</sub>O<sub>2</sub> decreases. The trend might indicate that efficient SO<sub>2</sub> oxidation via the O<sub>3</sub> reaction dominates at a high NH<sub>3</sub> emission ratio.

365 With O<sub>3</sub> in excess of SO<sub>2</sub>, [all](#) SO<sub>2</sub> is completely reacted. As NH<sub>3</sub> emission is reduced to less than 0.6~~x~~, the increased acidity significantly slows ~~down~~ SO<sub>2</sub> oxidation via the O<sub>3</sub> reaction, [causingand](#) the system [to switches](#) to H<sub>2</sub>O<sub>2</sub> oxidation.

~~Based on the observation trend, we can derive an initial condition of H<sub>2</sub>O<sub>2</sub>, O<sub>3</sub>, SO<sub>2</sub>, and sulfate for the box model under the assumption of SO<sub>2</sub> oxidation purely by ozone for control run and H<sub>2</sub>O<sub>2</sub> oxidation at NH<sub>3</sub> emission ratio = 0.2 (abbreviated as~~

"NH3\_02x run"). All other required parameters, such as the concentrations of total nitric acid and dust, are assumed as to be the same as those in the control run. Therefore, the initial conditions for the box model can be derived using H<sub>2</sub>O<sub>2</sub> concentration from the control run, the O<sub>3</sub> concentration from NH3\_02x run, and SO<sub>2</sub> concentration as SO<sub>2</sub> in NH3\_02x run, adjusted by adding H<sub>2</sub>O<sub>2</sub> difference between the control run and the NH3\_02x run to account for, considering the consumed SO<sub>2</sub> by the H<sub>2</sub>O<sub>2</sub> oxidation reaction. The initial value of SO<sub>4</sub> is calculated derived by subtracting the applied SO<sub>2</sub> initial concentration from the total S (i.e., PM-sulfate + SO<sub>2</sub> in the control run). A summary of the initial conditions is provided in Table S3.

Figure 6 shows the comparison between box model results and corresponding CMAQ results. Considering the main aqueous phase reactions involving O<sub>3</sub> and H<sub>2</sub>O<sub>2</sub>, the box model findings demonstrate that as the initial total NH<sub>3</sub> concentration decreases, the pH and H<sub>2</sub>O<sub>2</sub> also decrease, while SO<sub>2</sub> and O<sub>3</sub> increase. These trends are consistent with the pattern observed in CMAQ but with some discrepancies. Specifically, in the box model, the concentration of SO<sub>2</sub> tends to be slightly higher at lower NH<sub>3</sub> emission ratios, whereas the concentrations of H<sub>2</sub>O<sub>2</sub> and O<sub>3</sub> are lower than CMAQ results. Introducing additional oxidation reactions, i.e., the oxidation of tetravalent sulfur by O<sub>2</sub> with Fe(III) and Mn(II) catalysis in the system, brings the box model results closer to those of CMAQ. The box model demonstrates that higher NH<sub>3</sub> concentrations lead to higher pH values, resulting in O<sub>3</sub>-dominated chemistry. The reduction of NH<sub>3</sub> emissions can increase environmental acidity, slow O<sub>3</sub> oxidation reactions, and gradually transition to an H<sub>2</sub>O<sub>2</sub>-dominated condition. However, in the studied environment, the concentration of H<sub>2</sub>O<sub>2</sub> is lower than that of SO<sub>2</sub>, resulting in residual SO<sub>2</sub> once H<sub>2</sub>O<sub>2</sub> is depleted but causing a reduction in PM-sulfate.

### 3.5 Cost of emission reduction

The PM<sub>2.5</sub> reduction efficiency (Fig. 7a) based on the fitted trend fitted of in Fig. 3 increases as the emission ratio decreases across the three emission adjustment scenarios. In-Under the studied emission condition (i.e., emission ratio = 1), NH<sub>3</sub> reduction shows the highest reduction efficiency is for NH<sub>3</sub>, followed by SO<sub>2</sub> and with NOx having with the lowest. The increasing trend with the reduction ratio suggests an expected higher PM<sub>2.5</sub> reduction efficiency as the emission control policies continue. However, as discussed in Section 3.3, reducing SO<sub>2</sub> emissions has the least significant improvement in PM<sub>2.5</sub> levels. So, when the emission ratio is less than 0.8, its the emission reduction efficiency of SO<sub>2</sub> emissions is exceeded by that of reducing NOx emissions, indicating Hence, that the available reduction capacity of SO<sub>2</sub> is the lowest for SO<sub>2</sub>. Additionally, the PM<sub>2.5</sub> reduction efficiency during relatively clean period and high pollution period is presented in Figs. S12a and S13a, respectively. During the clean period (6<sup>th</sup> to 12<sup>th</sup> December), NH<sub>3</sub> reduction maintains the highest efficiency, followed by SO<sub>2</sub> and NOx. However, during the high pollution period (16<sup>th</sup> to 22<sup>thnd</sup> December), NH<sub>3</sub> reduction still has the highest efficiency, but NOx is higher than SO<sub>2</sub>. This indicates that during high pollution periods, reducing SO<sub>2</sub> emission has a limited effect on the total amount of PM<sub>2.5</sub> concentration, and continued reducing SO<sub>2</sub> emission does not improve efficiency. The average results of these two different conditions explain the crossover pattern observed for SO<sub>2</sub> and NOx emission reduction in Fig. 7a.

400 ~~In the aspect of~~Regarding policy considerations, cost becomes a crucial factor. Figs. 7b, S12b, and S13b illustrates the PM<sub>2.5</sub> reduction costs associated with these emission reduction experiments. ~~We focus on the average results for December (Fig. 7b).~~ ~~The~~ reduction of NO<sub>x</sub> emissions incurs the highest cost, amounting to approximately one billion dollars ~~yr<sup>-1</sup>~~per year to achieve a 1 µg m<sup>-3</sup> reduction in PM<sub>2.5</sub> concentration. In comparison, the cost of SO<sub>2</sub> emission reduction ranges from tens of millions to 100 million dollars ~~per year~~yr<sup>-1</sup>, while NH<sub>3</sub> emission reduction costs are around fifty million dollars ~~per year~~yr<sup>-1</sup>. Therefore, performing NH<sub>3</sub> and SO<sub>2</sub> emission reductions would be more cost-efficient ~~in for~~ achieving a PM<sub>2.5</sub> reduction. However, cost evaluation involves uncertainties. Kaminski (2003) approach to estimating MAC of SO<sub>2</sub> focuses on power plants, discussing costs tied to emission control through alternative energy sources or equipment enhancements. On the other hand, Gu et al. (2021) employed the online Greenhouse Gas and Air Pollution Interactions and Synergies (GAINS) model to comprehensively assess the MAC of reducing NO<sub>x</sub> and NH<sub>3</sub> emissions across five continents and globally. Applying these methods to Taiwan may encounter uncertainties due to varying energy mixes, industrial structures, and environmental conditions in different regions. ~~Such-These~~ distinctions could diverge from ~~prior~~previous study assumptions, affecting the cost-effectiveness of emission reduction strategies. Additional factors, including meteorological patterns and technological landscapes, may introduce uncertainties in cost estimations.

405 Furthermore, our study assumed a constant MAC value. In reality, MAC may vary as emissions decrease, usually becoming more expensive. Varied emission reduction approaches could result in substantial cost disparities, demanding careful consideration for regional applications. Therefore, a more comprehensive cost-benefit analysis, accounting for regional variations and potential changes in MAC with emission reduction, is crucial to devise effective and economically viable air pollution control strategies.

#### 4 Conclusion

420 This study ~~investigated~~investigates the impacts of emission reduction on PM<sub>2.5</sub> and the secondary inorganic components (sulfate, nitrate, and ammonium) while assessing the effectiveness of emission reduction strategies in central Taiwan using the CMAQ model ~~during for~~ December 2018. In our simulations, the mean PM<sub>2.5</sub> concentration in central Taiwan ~~is was~~ 21.1 µg m<sup>-3</sup>, ~~comprising~~including 2.7 µg m<sup>-3</sup> of sulfate, 6.3 µg m<sup>-3</sup> of nitrate, 2.6 µg m<sup>-3</sup> of ammonium and other species including organics. For sulfate, 43.7% comes from chemical processes, with 30.5% from aqueous reactions and 13.2% from gas-phase reactions.

425 In ~~the evaluation~~of emission reduction strategies, it was observed that ~~the impact of reducing~~ SO<sub>2</sub> emission ~~has a less significant reduction impact~~ on mitigating PM<sub>2.5</sub> ~~was less significant~~ compared to reductions in NO<sub>x</sub> and NH<sub>3</sub> emissions. This is attributed to the fact that SO<sub>2</sub> emission reduction primarily affects sulfate, which constitutes only 12% of PM<sub>2.5</sub> in this ~~studied case~~study. On the other hand, ~~the~~ reductions of NO<sub>x</sub> or NH<sub>3</sub> emission ~~led to~~substantially ~~contributed to a significant~~ decreases in nitrate and ammonium, effectively mitigating PM<sub>2.5</sub>. However, a non-linear effect ~~exists~~was noted between the ~~emission~~reductions of NO<sub>x</sub> and NH<sub>3</sub> emissions, indicating that ~~the~~ mitigating effects of these two emissions are not linearly

additive. Through sensitivity analysis, the ~~impact reduction~~ of NO<sub>x</sub> or NH<sub>3</sub> emission ~~reduction on PM<sub>2.5</sub>~~ is relatively ~~close similar~~ in northern Taiwan, Chu-Miao area, and central Taiwan. ~~While the Yun-Chia-Nan area and Kao-Ping area show a preference for~~ NO<sub>x</sub> emission reduction. Notably, NH<sub>3</sub> emission reduction affects sulfur chemical reactions in the aqueous phase through changing pH values in cloud droplets, ~~switching-shifting~~ the primary oxidant from ozone to H<sub>2</sub>O<sub>2</sub>, which is a limited agent in this ~~studied case study~~. The sensitivity of the ~~S(IV) to S(VI) oxidation reaction of S(IV) to S(VI) with respect~~ to acidity was verified using ~~the a~~ box model. The oxidations by O<sub>2</sub> catalyzed via Fe(III) and Mn(II) were also ~~confirmed found to have a significant contributions significantly contribute~~ to the ~~sulfur oxidation processes~~, as demonstrated ~~using a by the~~ box model. Other research ~~has highlighted also indicated~~ the importance of metal ion-catalyzed sulfur oxidation reactions ~~for in the generation of sulfate formation, with. In winter,~~ this pathway ~~can contribute inge~~ up to 19% of sulfate formation in China ~~during winter~~ (Huang et al., 2014).

Emission reduction strategies to combat PM<sub>2.5</sub> are crucial but entail considerable costs. Our comprehensive analysis ~~reveals shows~~ that, considering both efficiency and cost, reducing NH<sub>3</sub> emissions ~~emerges as~~ the most effective strategy for the studied Taiwan's environmental conditions. However, it is imperative to acknowledge that NH<sub>3</sub> emissions are mainly associated with industrial, agricultural, and livestock activities. Industrial ammonia manufacturing has ~~historically boosted greatly increased~~ global food production and population ~~in the past~~ (Erismann et al., 2008), and green ammonia may also play a significant role in future carbon-free energy endeavors (Chehade et al., 2021; Kang et al., 2015). Therefore, exploring large-scale emission reduction strategies and carefully assessing potential issues, such as aerosol pH changes leading to increased acid rain (Liu et al., 2019), are vital areas for further research. Overall, this study provides valuable insights into the intricate interactions among air pollutants and their impacts on PM<sub>2.5</sub>, highlighting the ongoing need for continued efforts to reduce emissions and improve air quality in Taiwan.

### Code availability

The code is not publicly accessible, but readers can contact HM Hung (hnhung@ntu.edu.tw) for more information.

### Data availability

The CMAQ model output and TW-MOENV observation data used in this study can be accessed online at <https://doi.org/10.5281/zenodo.10623526>.

## Author contributions

PC Huang set up experiments, ran experiments, and prepared the draft. HM Hung supervised the project, including data discussion and manuscript editing. HC Lai provided the control run of WRF and CMAQ model. CCK Chou provided IC  
460 analysis of PM<sub>2.5</sub>.

## Competing interests

The authors declare that they have no conflict of interest.

## Acknowledgments

This study is supported by National Science and Technology Council (NSTC), Taiwan under grants of 111-2111-M-002-009  
465 and 112-2111-M-002-014. We acknowledge the valuable insights from Dr. Ruijun Dang at Harvard and Prof. Jen-Ping Chen at National Taiwan University for the sensitivity analysis discussion.

## References

- Byun, D., and Schere, K. L.: Review of the Governing Equations, Computational Algorithms, and Other Components of the Models-3 Community Multiscale Air Quality (CMAQ) Modeling System, *Appl. Mech. Rev.*, 59, 51-77, 10.1115/1.2128636,  
470 2006.
- Chehade, G., and Dincer, I.: Progress in green ammonia production as potential carbon-free fuel, *Fuel*, 299, 120845, <https://doi.org/10.1016/j.fuel.2021.120845>, 2021.
- Chen, C.-L., Chen, T.-Y., Hung, H.-M., Tsai, P.-W., Chou, C. C. K., and Chen, W.-N.: The influence of upslope fog on hygroscopicity and chemical composition of aerosols at a forest site in Taiwan, *Atmos. Environ.*, 246, 118150,  
475 <https://doi.org/10.1016/j.atmosenv.2020.118150>, 2021.
- Chen, Y., Shen, H., and Russell, A. G.: Current and Future Responses of Aerosol pH and Composition in the U.S. to Declining SO<sub>2</sub> Emissions and Increasing NH<sub>3</sub> Emissions, *Environ. Sci. Technol.*, 53, 9646-9655, 10.1021/acs.est.9b02005, 2019.
- Cheng, F.-Y., and Hsu, C.-H.: Long-term variations in PM<sub>2.5</sub> concentrations under changing meteorological conditions in Taiwan, *Sci. Rep.*, 9, 6635, 10.1038/s41598-019-43104-x, 2019.
- 480 Chuang, M.-T., Chou, C. C. K., Hsiao, T.-C., Lin, K.-y., Lin, N.-H., Lin, W.-Y., Wang, S.-H., Pani, S. K., and Lee, C.-T.: Analyzing the increasing importance of nitrate in Taiwan from long-term trend of measurements, *Atmos. Environ.*, 267, 118749, <https://doi.org/10.1016/j.atmosenv.2021.118749>, 2021.



- Derwent, R., Witham, C., Redington, A., Jenkin, M., Stedman, J., Yardley, R., and Hayman, G.: Particulate matter at a rural location in southern England during 2006: Model sensitivities to precursor emissions, *Atmos. Environ.*, 43, 689-696, <https://doi.org/10.1016/j.atmosenv.2008.09.077>, 2009.
- 485
- Erisman, J. W., Sutton, M. A., Galloway, J., Klimont, Z., and Winiwarter, W.: How a century of ammonia synthesis changed the world, *Nature Geoscience*, 1, 636-639, 10.1038/ngeo325, 2008.
- Gu, B., Zhang, L., Van Dingenen, R., Vieno, M., Van Grinsven, H. J. M., Zhang, X., Zhang, S., Chen, Y., Wang, S., Ren, C., Rao, S., Holland, M., Winiwarter, W., Chen, D., Xu, J., and Sutton, M. A.: Abating ammonia is more cost-effective than
- 490 nitrogen oxides for mitigating PM<sub>2.5</sub> air pollution, *Science*, 374, 758-762, 10.1126/science.abf8623, 2021.
- Hsieh, M.-K., Chen, Y.-W., Chen, Y.-C., and Wu, C.-M.: The Roles of Local Circulation and Boundary Layer Development in Tracer Transport over Complex Topography in Central Taiwan, *Journal of the Meteorological Society of Japan. Ser. II*, 100, 555-573, 10.2151/jmsj.2022-028, 2022.
- Hsu, C.-H., and Cheng, F.-Y.: Classification of weather patterns to study the influence of meteorological characteristics on
- 495 PM<sub>2.5</sub> concentrations in Yunlin County, Taiwan, *Atmos. Environ.*, 144, 397-408, <https://doi.org/10.1016/j.atmosenv.2016.09.001>, 2016.
- Hu, J., Chen, J., Ying, Q., and Zhang, H.: One-year simulation of ozone and particulate matter in China using WRF/CMAQ modeling system, *Atmos. Chem. Phys.*, 16, 10333-10350, 10.5194/acp-16-10333-2016, 2016.
- Huang, X., Song, Y., Zhao, C., Li, M., Zhu, T., Zhang, Q., and Zhang, X.: Pathways of sulfate enhancement by natural and
- 500 anthropogenic mineral aerosols in China, *J. Geophys. Res. Atmos.*, 119, 14,165-114,179, <https://doi.org/10.1002/2014JD022301>, 2014.
- IPCC: Climate Change 2021: The Physical Science Basis. Contribution of Working Group I to the Sixth Assessment Report of the Intergovernmental Panel on Climate Change, edited by: Masson-Delmotte, V., Zhai, P., Pirani, A., Connors, S. L., Péan, C., Berger, S., Caud, N., Chen, Y., Goldfarb, L., Gomis, M. I., Huang, M., Leitzell, K., Lonnoy, E., Matthews, J. B. R.,
- 505 Maycock, T. K., Waterfield, T., Yelekçi, O., Yu, R., and Zhou, B., Cambridge University Press, Cambridge, United Kingdom and New York, NY, USA, 2021.
- Jacobson, M. Z.: Development and application of a new air pollution modeling system—II. Aerosol module structure and design, *Atmos. Environ.*, 31, 131-144, [https://doi.org/10.1016/1352-2310\(96\)00202-6](https://doi.org/10.1016/1352-2310(96)00202-6), 1997.
- Kaminski, J.: Technologies and costs of SO<sub>2</sub>-emissions reduction for the energy sector, *Appl. Energy*, 75, 165-172, [https://doi.org/10.1016/S0306-2619\(03\)00029-1](https://doi.org/10.1016/S0306-2619(03)00029-1), 2003.
- 510
- Kang, D. W., and Holbrook, J. H.: Use of NH<sub>3</sub> fuel to achieve deep greenhouse gas reductions from US transportation, *Energy Reports*, 1, 164-168, <https://doi.org/10.1016/j.egyr.2015.08.001>, 2015.
- Lai, H.-C., and Lin, M.-C.: Characteristics of the upstream flow patterns during PM<sub>2.5</sub> pollution events over a complex island topography, *Atmos. Environ.*, 227, 117418, <https://doi.org/10.1016/j.atmosenv.2020.117418>, 2020.

- 515 Lee, C. S. L., Chou, C. C. K., Cheung, H. C., Tsai, C. Y., Huang, W. R., Huang, S. H., Chen, M. J., Liao, H. T., Wu, C. F., Tsao, T. M., Tsai, M. J., and Su, T. C.: Seasonal variation of chemical characteristics of fine particulate matter at a high-elevation subtropical forest in East Asia, *Environ. Pollut.*, 246, 668-677, <https://doi.org/10.1016/j.envpol.2018.11.033>, 2019.
- Liu, M., Huang, X., Song, Y., Tang, J., Cao, J., Zhang, X., Zhang, Q., Wang, S., Xu, T., Kang, L., Cai, X., Zhang, H., Yang, F., Wang, H., Yu, J. Z., Lau, A. K. H., He, L., Huang, X., Duan, L., Ding, A., Xue, L., Gao, J., Liu, B., and Zhu, T.: Ammonia emission control in China would mitigate haze pollution and nitrogen deposition, but worsen acid rain, *Proc. Natl. Acad. Sci. U.S.A.*, 116, 7760-7765, doi:10.1073/pnas.1814880116, 2019.
- Maynard, A. D., and Maynard, R. L.: A derived association between ambient aerosol surface area and excess mortality using historic time series data, *Atmos. Environ.*, 36, 5561-5567, [https://doi.org/10.1016/S1352-2310\(02\)00743-4](https://doi.org/10.1016/S1352-2310(02)00743-4), 2002.
- Petetin, H., Sciare, J., Bressi, M., Gros, V., Rosso, A., Sanchez, O., Sarda-Estève, R., Petit, J. E., and Beekmann, M.: Assessing the ammonium nitrate formation regime in the Paris megacity and its representation in the CHIMERE model, *Atmos. Chem. Phys.*, 16, 10419-10440, 10.5194/acp-16-10419-2016, 2016.
- 525 Ramanathan, V., Crutzen, P. J., Kiehl, J. T., and Rosenfeld, D.: Aerosols, Climate, and the Hydrological Cycle, *Science*, 294, 2119-2124, 10.1126/science.1064034, 2001.
- Redington, A. L., Derwent, R. G., Witham, C. S., and Manning, A. J.: Sensitivity of modelled sulphate and nitrate aerosol to cloud, pH and ammonia emissions, *Atmos. Environ.*, 43, 3227-3234, <https://doi.org/10.1016/j.atmosenv.2009.03.041>, 2009.
- Schroder, J., Campuzano-Jost, P., Day, D., Shah, V., Sullivan, A., Campos, T., Reeves, J., Hills, A., Guo, H., Fibiger, D., McDuffie, E., Weber, R., Apel, E., Jaeglé, L., Brown, S., Thornton, J., and Jimenez, J.: Sources and Secondary Production of Organic Aerosols in the Northeastern United States during WINTER, *J. Geophys. Res. Atmos.*, 123, 10.1029/2018JD028475, 2018.
- 535 Seinfeld, J. H., and Pandis, S. N.: *Atmospheric Chemistry and Physics: From Air Pollution to Climate Change*, Wiley, 2006.
- Shiraiwa, M., Ueda, K., Pozzer, A., Lammel, G., Kampf, C. J., Fushimi, A., Enami, S., Arangio, A. M., Fröhlich-Nowoisky, J., Fujitani, Y., Furuyama, A., Lakey, P. S. J., Lelieveld, J., Lucas, K., Morino, Y., Pöschl, U., Takahama, S., Takami, A., Tong, H., Weber, B., Yoshino, A., and Sato, K.: *Aerosol Health Effects from Molecular to Global Scales*, *Environ. Sci. Technol.*, 51, 13545-13567, 10.1021/acs.est.7b04417, 2017.
- 540 Skamarock, W. C., Klemp, J. B., Dudhia, J., Gill, D. O., Barker, D. M., Duda, M. G., Huang, X., Wang, W., and Powers, J. G.: *A Description of the Advanced Research WRF Version 3*, U.S. National Center for Atmospheric Research, Boulder, Colorado, NCAR/TN-475+STR, 2008.
- Sugiyama, T., Ueda, K., Seposo, X. T., Nakashima, A., Kinoshita, M., Matsumoto, H., Ikemori, F., Honda, A., Takano, H., Michikawa, T., and Nitta, H.: Health effects of PM<sub>2.5</sub> sources on children's allergic and respiratory symptoms in Fukuoka, Japan, *Sci. Total Environ.*, 709, 136023, <https://doi.org/10.1016/j.scitotenv.2019.136023>, 2020.
- 545 Takahama, S., Wittig, A. E., Vayenas, D. V., Davidson, C. I., and Pandis, S. N.: Modeling the diurnal variation of nitrate during the Pittsburgh Air Quality Study, *J. Geophys. Res. Atmos.*, 109, D16S06, 10.1029/2003JD004149, 2004.

- Tsimpidi, A. P., Karydis, V. A., and Pandis, S. N.: Response of Inorganic Fine Particulate Matter to Emission Changes of Sulfur Dioxide and Ammonia: The Eastern United States as a Case Study, *J. Air Waste Manage. Assoc.*, 57, 1489-1498, 10.3155/1047-3289.57.12.1489, 2007.
- 550 Veratti, G., Stortini, M., Amorati, R., Bressan, L., Giovannini, G., Bande, S., Bissardella, F., Ghigo, S., Angelino, E., Colombo, L., Fossati, G., Malvestiti, G., Marongiu, A., Dalla Fontana, A., Intini, B., and Pillon, S.: Impact of NO<sub>x</sub> and NH<sub>3</sub> Emission Reduction on Particulate Matter across Po Valley: A LIFE-IP-PREPAIR Study, *Atmosphere*, 14, 10.3390/atmos14050762, 2023.
- 555 Vohra, K., Marais, E. A., Bloss, W. J., Schwartz, J., Mickley, L. J., Van Damme, M., Clarisse, L., and Coheur, P.-F.: Rapid rise in premature mortality due to anthropogenic air pollution in fast-growing tropical cities from 2005 to 2018, *Science Advances*, 8, eabm4435, 10.1126/sciadv.abm4435, 2022.
- WHO: Review of evidence on health aspects of air pollution: REVIHAAP project: technical report, World Health Organization. Regional Office for Europe, Copenhagen, 2021.
- 560 Wyatt Appel, K., Napelenok, S., Hogrefe, C., Pouliot, G., Foley, K. M., Roselle, S. J., Pleim, J. E., Bash, J., Pye, H. O. T., Heath, N., Murphy, B., and Mathur, R.: Overview and Evaluation of the Community Multiscale Air Quality (CMAQ) Modeling System Version 5.2, *Air Pollution Modeling and its Application XXV*, Cham, 2018.
- Zhang, Q., Jimenez, J. L., Worsnop, D. R., and Canagaratna, M.: A Case Study of Urban Particle Acidity and Its Influence on Secondary Organic Aerosol, *Environ. Sci. Technol.*, 41, 3213-3219, 10.1021/es061812j, 2007.

565

## Tables

**Table 1: Experimental design.**

<b>Experiments</b>	<b>Descriptions</b>
<b>Control run</b>	Use mechanism cb6r3ae6aq
<b>NoAqChem run</b>	Turn off sulfur aqueous phase oxidation reactions
<b>NoChem run</b>	Turn off all chemistry reactions
<b>ER1 runs</b>	SO <sub>2</sub> , NO <sub>x</sub> , and NH <sub>3</sub> emissions reduced by ratios of 0.8, 0.6, 0.4, and 0.2 separately
<b>ER2 runs</b>	Both NO <sub>x</sub> , and NH <sub>3</sub> emissions reduced by ratios of 0.8, 0.6, 0.4, and 0.2 (only 12/1~12/14)
<b>EI runs</b>	SO <sub>2</sub> , NO <sub>x</sub> , and NH <sub>3</sub> emissions increased by ratios of 1.5 and 2.0 separately

570 **Table 2: The applied chemical reactions related to the formation of sulfate, nitrate, and ammonium.**

	<b>Reaction</b>
<b>Gas phase</b>	1. $\text{SO}_{2(\text{g})} + \text{OH}_{(\text{g})} \rightarrow \text{HSO}_{3(\text{g})} \rightarrow \text{H}_2\text{SO}_{4(\text{g})}$
	2. $\text{NO}_{2(\text{g})} + \text{OH}_{(\text{g})} \rightarrow \text{HNO}_{3(\text{g})}$
	3. $\text{N}_2\text{O}_{5(\text{g})} + \text{H}_2\text{O} \rightarrow 2\text{HNO}_{3(\text{g})}$
<b>Aqueous phase</b>	4. $\text{H}_2\text{SO}_{4(\text{aq})} \rightarrow \text{SO}_{4(\text{aq})}^{2-} + 2\text{H}^+$
	5. $\text{S}(\text{IV})_{(\text{aq})} + \text{Oxidants}_{(\text{aq})} \rightarrow \text{SO}_4^{2-} + 2\text{H}^+$ * S(IV): $\text{H}_2\text{SO}_3, \text{HSO}_3^-, \text{SO}_3^{2-}$ * Oxidants: $\text{O}_3, \text{H}_2\text{O}_2, \text{MHP}, \text{PAA}, \text{O}_2$
	6. $\text{NH}_{3(\text{g})} \leftrightarrow \text{NH}_{3(\text{aq})} \leftrightarrow \text{NH}_4^+_{(\text{aq})} + \text{OH}^-$
	7. $\text{HNO}_{3(\text{g})} \leftrightarrow \text{HNO}_{3(\text{aq})} \leftrightarrow \text{NO}_3^-_{(\text{aq})} + \text{H}^+$
	8. $\text{H}^+ + \text{OH}^- \rightarrow \text{H}_2\text{O}$

**Table 3: Statistic of wind and PM<sub>2.5</sub> of MOENV observation and model simulation for four stations.**

	Tamsui	Shalu	Taixi	Qianzhen	<sup>a</sup> Criteria
<b>Wind speed (m/s)</b>					
Mean value of MOENV	1.99	4.52	7.52	2.07	
Mean value of WRF	3.25	4.73	4.85	2.33	
Correlation coefficient	0.46	0.85	0.69	0.42	
Mean bias error	1.22	0.21	-2.70	0.25	≤ ±0.5
Mean absolute error	1.56	1.11	3.00	0.77	≤ 2.0
<b>PM<sub>2.5</sub> concentration (µg m<sup>-3</sup>)</b>					
Mean value of MOENV	10.75	16.09	20.93	31.72	
Mean value of CMAQ	12.12	19.70	15.97	40.56	
Correlation coefficient	0.59	0.70	0.71	0.42	
Mean bias error	1.42	3.72	-4.79	8.88	
Mean absolute error	8.02	9.36	10.37	15.02	
Mean fractional bias	-0.32	0.21	-0.48	0.19	≤ ±0.6
Mean fractional error	0.71	0.56	0.66	0.40	≤ 0.75

<sup>a</sup>The criteria are suggested by Hu et al. (2016).

575 Correlation coefficient = 
$$\frac{\sum_{i=1}^n (m_i - \bar{m})(o_i - \bar{o})}{\sqrt{\sum_{i=1}^n (m_i - \bar{m})^2} \sqrt{\sum_{i=1}^n (o_i - \bar{o})^2}}$$

Mean bias error =  $(m_i - o_i)$

Mean absolute error =  $|m_i - o_i|$

Mean fractional bias =  $2 \times \left( \frac{m_i - o_i}{m_i + o_i} \right)$

Mean fractional error =  $2 \times \left| \left( \frac{m_i - o_i}{m_i + o_i} \right) \right|$

580 where  $m_i$  and  $o_i$  are the wind speed or concentrations of model and observation at time  $i$ , respectively, and  $\bar{m}$  and  $\bar{o}$  are the average values over December 2018.

**Table 4: Correlation coefficients of PM<sub>2.5</sub>, sulfate, nitrate, ammonium, and meteorological parameters (WS and QC) of control run for central Taiwan.**

	PM <sub>2.5</sub>	SO <sub>4</sub> <sup>2-</sup>	NO <sub>3</sub> <sup>-</sup>	NH <sub>4</sub> <sup>+</sup>	dSO <sub>4</sub> <sup>2-</sup>
SO <sub>4</sub> <sup>2-</sup>	0.65	-	-	-	0.73
NO <sub>3</sub> <sup>-</sup>	0.97	0.61	-	-	-
NH <sub>4</sub> <sup>+</sup>	0.95	0.77	0.98	-	-
WS	-0.54	-0.34	-0.51	-0.52	-
QC	0.05	0.43	0.07	0.18	0.65

585 WS is the single-point wind speed of the surface layer in Shalu.

QC is the average cloud water within the planetary boundary layer in central Taiwan.

dSO<sub>4</sub><sup>2-</sup> is the sulfate difference concentration (control run – NoAqChem run).

**Table 5: Statistics of pH in cloud droplets and the concentration of gaseous components in both land (32130 grid points) and sea (122316 grid points) regions.**

Variables	Land			Sea		
	Mean	Q1	Q3	Mean	Q1	Q3
<b>pH</b>	5.15	5.00	5.00	5.01	5.00	5.00
<b>SO<sub>2</sub> (ppbv)</b>	1.65	1.01	1.96	1.68	1.16	1.90
<b>NH<sub>3</sub> (ppbv)</b>	2.10	0.03	0.84	0.42	0.02	0.16
<b>HNO<sub>3</sub> (ppbv)</b>	0.37	0.11	0.51	1.42	0.61	1.72
<b>H<sub>2</sub>O<sub>2</sub> (ppbv)</b>	0.06	0.003	0.06	0.05	0.002	0.03
<b>O<sub>3</sub> (ppbv)</b>	44.6	38.9	51.3	48.2	43.2	53.6

590 Mean: Arithmetic mean; Q1: 25th percentile; Q3: 75th percentile.



Figures

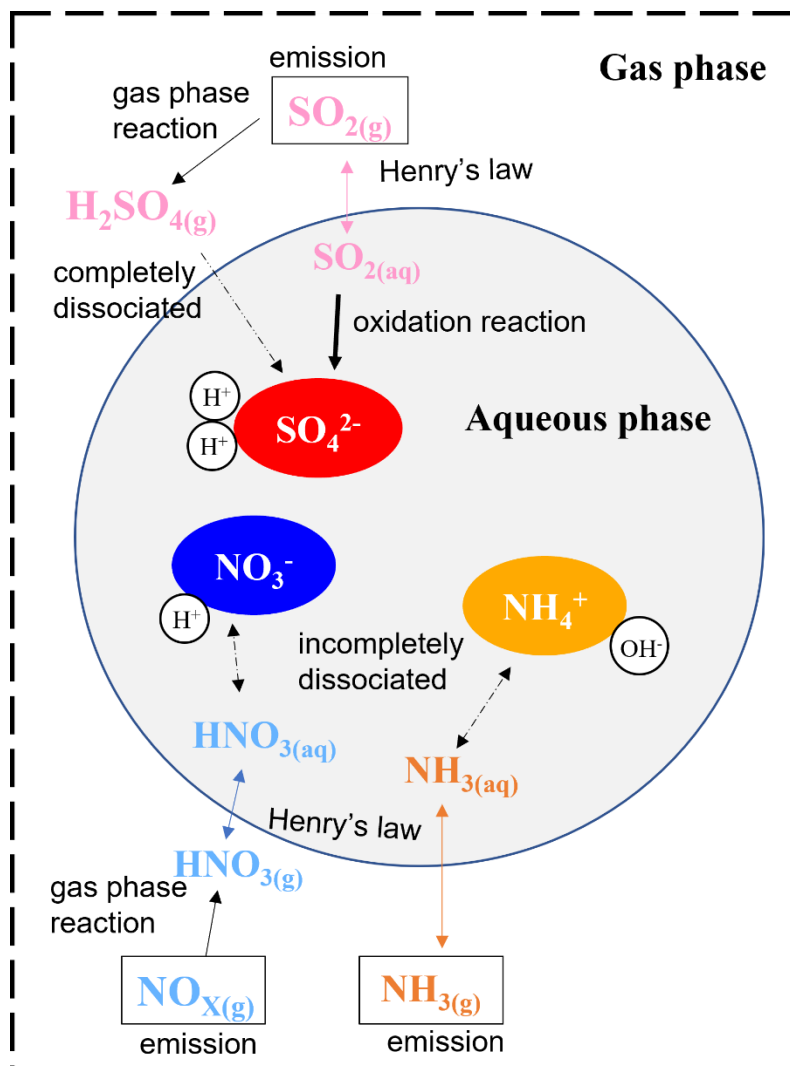
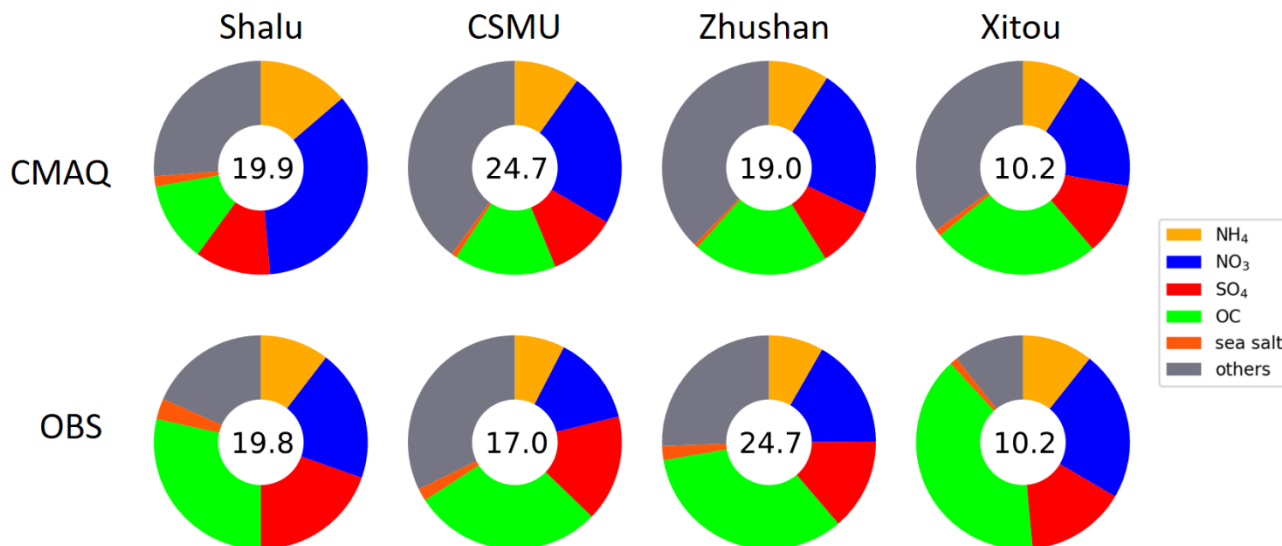
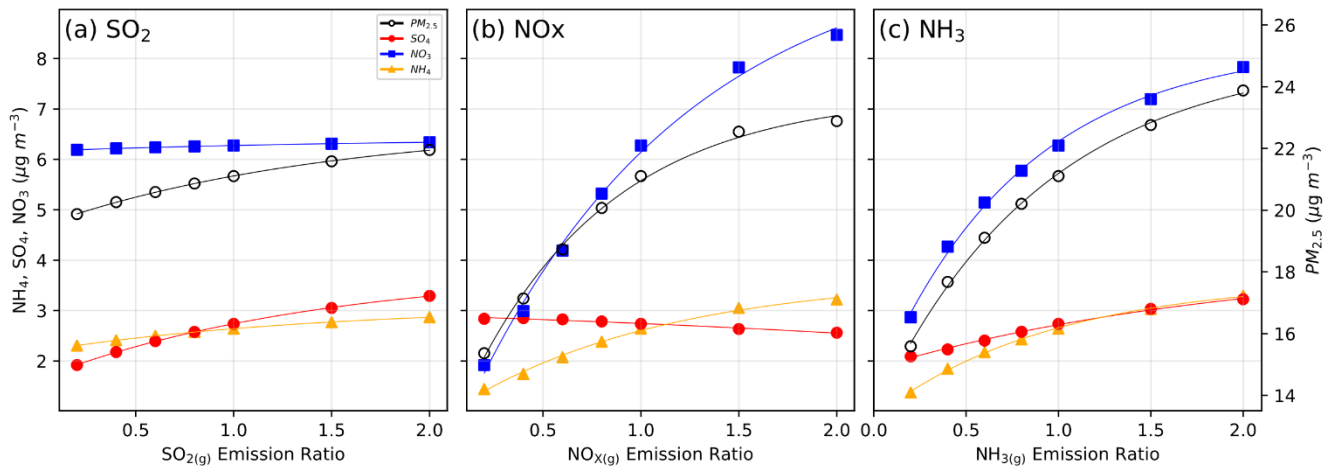


Figure 1: Schematic diagram of chemical interactions ~~for~~ in sulfate-nitrate-ammonium formation.

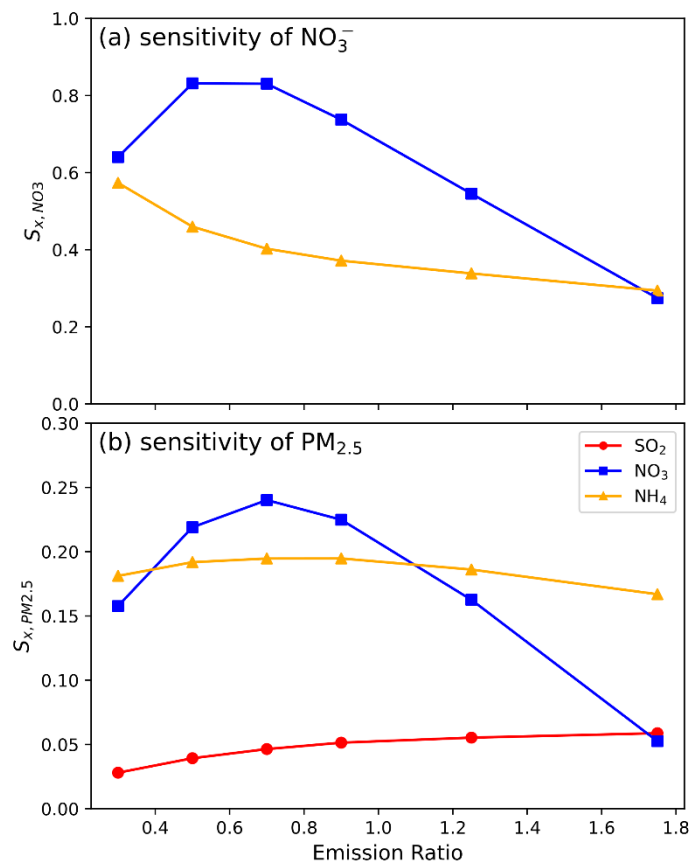


595 **Figure 2: The eC**omparison of PM<sub>2.5</sub> components **(the PM<sub>2.5</sub> concentration is indicated as a number inside the circle, μg m<sup>-3</sup>)** between intensive observation data and CMAQ surface layer data for four sites **(PM<sub>2.5</sub> concentration indicated inside the circle in μg m<sup>-3</sup>)**. **I**he individual **composition components are** shown in the legend, with colors arranged **in a in a** clockwise direction **starting** from the top. Conditions: mean values from 1<sup>st</sup> to 21<sup>st</sup> December 2018 for each station (OBS) or grid point (CMAQ).



600

Figure 3: The response of  $PM_{2.5}$  and major secondary inorganic components (sulfate, nitrate, and ammonium) to the emission ratio of (a)  $SO_2$ , (b)  $NO_x$ , and (c)  $NH_3$ . Lines are ~~applied to the fitting results - the data~~ using an exponential function. Conditions: averaged data ~~offor-central-Taiwan from 1-31 December 2018 for at~~ the surface layer of central Taiwan.



605

Figure 4: (a) Nitrate sensitivity coefficient of emission ratio for  $NO_x$  ( $S_{NO_x, NO_3}$ ) and  $NH_3$  ( $S_{NH_3, NO_3}$ ) and (b)  $PM_{2.5}$  sensitivity as a function coefficient of emission ratio for  $SO_2$  ( $S_{SO_2, PM_{2.5}}$ ),  $NO_x$  ( $S_{NO_x, PM_{2.5}}$ ) and  $NH_3$  ( $S_{NH_3, PM_{2.5}}$ ) as a function of emission ratio. Points Data are calculated using the first-order difference, with the x-axis representing the mean values of the two points involved in the differencing process. Conditions: averaged data for central Taiwan from 1-31 December 2018 for at the surface layer of central Taiwan.

610

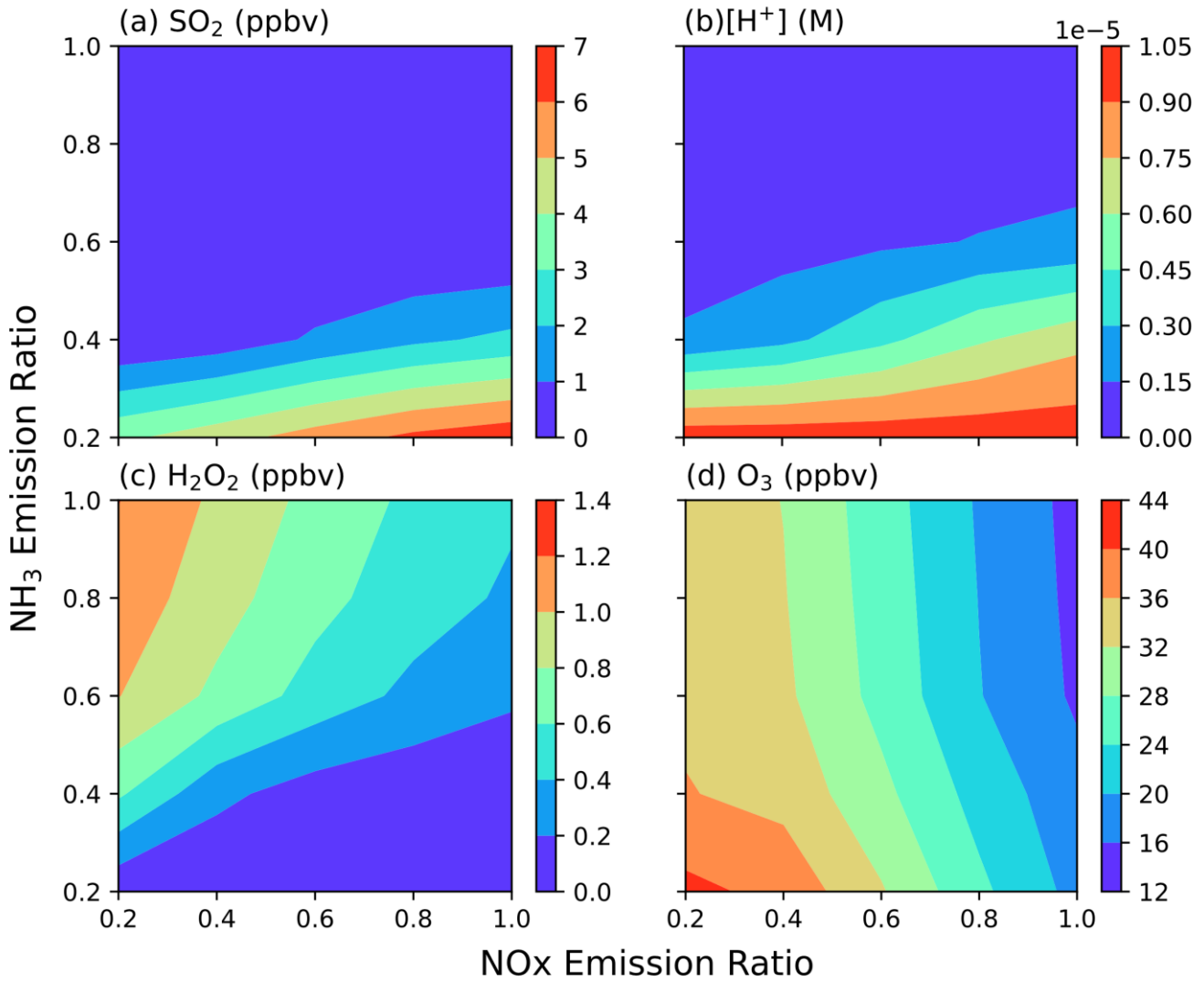


Figure 5: (a) SO<sub>2</sub>, (b) ~~hydrogen ion~~H<sup>+</sup>, (c) H<sub>2</sub>O<sub>2</sub>, and (d) ~~O<sub>3</sub>ozone~~ concentrations as a function of NO<sub>x</sub> (x-axis) and NH<sub>3</sub> (y-axis) emission ratios for a single grid point. Conditions: ~~data for 08:00 am LT on 3<sup>rd</sup> December 2018~~08:00 LT, ~~at an altitude of 68.5 m a.s.l. for the location of (24.2° N, 120.5° E),~~with an altitude of 68.5m above sea level.

615

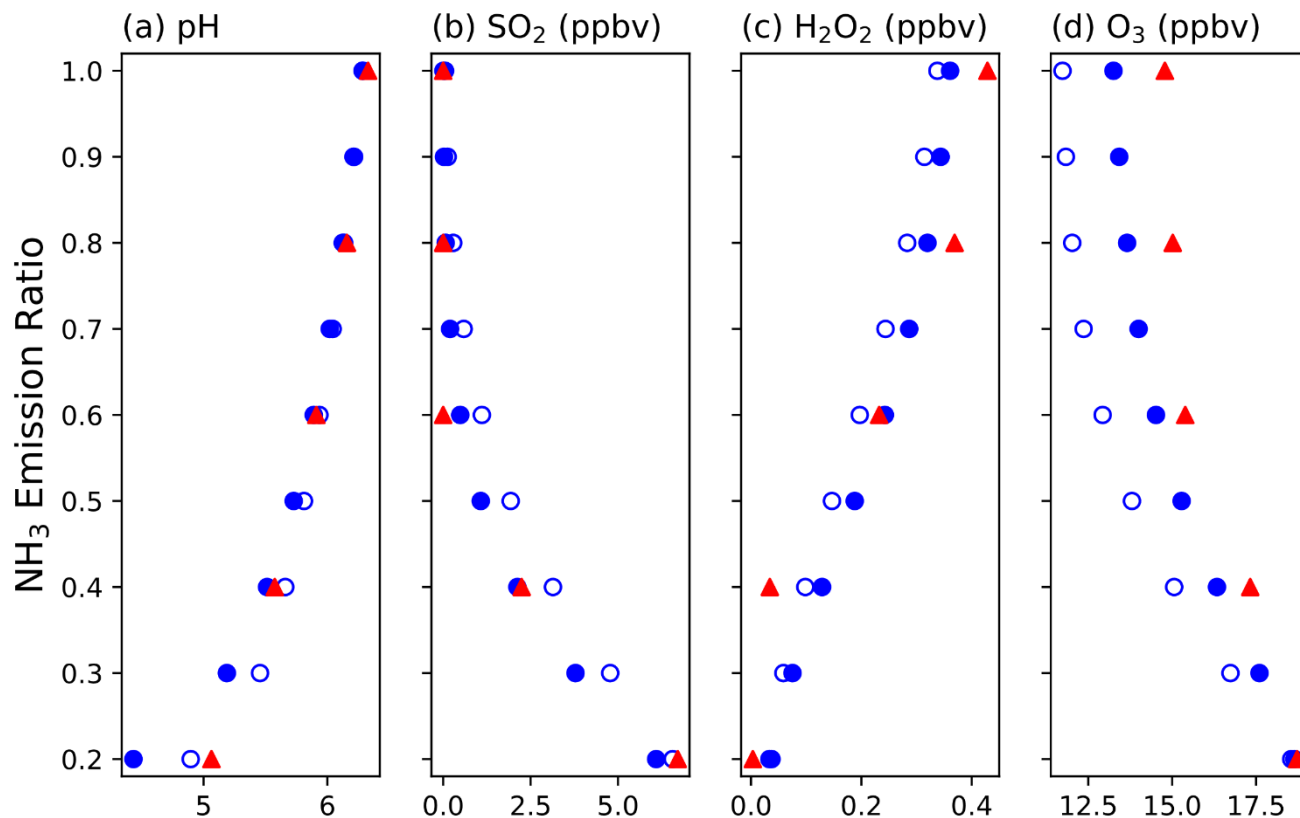


Figure 6: The comparison between CMAQ and box model results for (a) pH and the concentrations of (b) SO<sub>2</sub>, (c) H<sub>2</sub>O<sub>2</sub>, and (d) O<sub>3</sub> ozone as a function of NH<sub>3</sub> emission reduction ratio. Red triangle points: CMAQ model results; blue open circles: box model with H<sub>2</sub>O<sub>2</sub> and O<sub>3</sub> reactions; blue solid circles: box model with H<sub>2</sub>O<sub>2</sub>, O<sub>3</sub>, and O<sub>2</sub> catalyzed by Fe(III) and Mn(II) reactions.

620

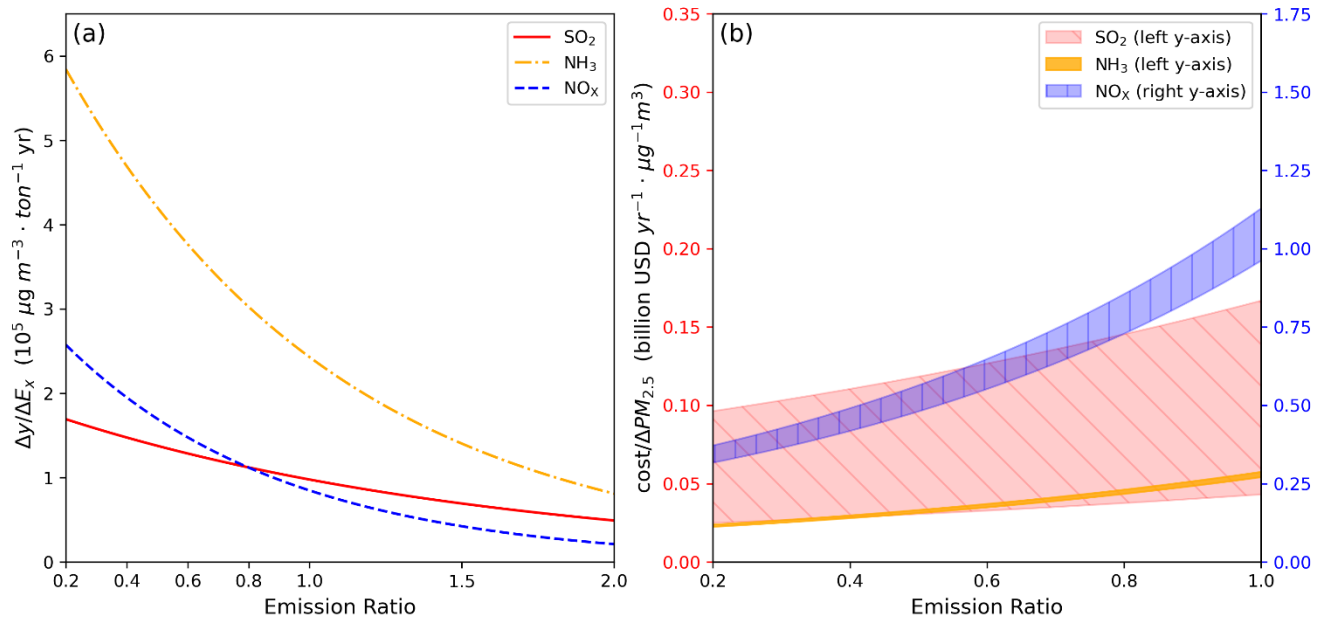


Figure 7: (a) PM<sub>2.5</sub> reduction efficiency and (b) reduction cost as a function of emission ratio for SO<sub>2</sub>, NH<sub>3</sub>, and NO<sub>x</sub>.

Supplementary Material for

5                    **Assessing the Effectiveness of SO<sub>2</sub>, NO<sub>x</sub>, and NH<sub>3</sub> Emission Reductions  
in Mitigating Winter PM<sub>2.5</sub> in Taiwan Using CMAQ Model**

by

10                   Ping-Chieh Huang<sup>1</sup>, Hui-Ming Hung<sup>1\*</sup>, Hsin-Chih Lai<sup>2</sup>, and Charles C.-K. Chou<sup>3</sup>

**Contents of this file**

15

Description of the relationship between  $S_{NO_x,NO_3}$  and NO<sub>2</sub> concentration

Tables S1 to S7

Figures S1 to S14†



20 **Relationship between  $S_{NO_x,NO_3}$  and  $NO_2$  concentration**

The reduction in  $NO_x$  emissions ~~induces~~ leads to a decrease in  $NO_2$  concentration, subsequently leading to a subsequent ~~reduction in~~ reduction in  $HNO_3$  production through reaction R1:



The production rate of  $HNO_3$  ( $P_{HNO_3}$ ) can be calculated ~~with~~ by assuming that  $OH$  concentration

25 ~~assumed is~~ in the steady state as follows:

$$\frac{d[OH]}{dt} = P_r - L = P - \sum k_i[A]_i [OH] - k_{NO_2}[NO_2][OH], \quad (1)$$

where  $P_r$  and  $L$  are chemical production and loss of  $[OH]$ , respectively,  $\sum k_i[A]_i [OH]$  is the sum of reaction rates of all  $OH$ -consuming chemical reactions except reaction (R1),  $k_i$  is the rate constant of each reaction.

30 The steady-state  $[OH]$  is estimated as follows:

$$[OH]_{SS} = \frac{P_r}{\sum k_i[A]_i + k_{NO_2}[NO_2]} \quad (2)$$

Thus, the production rate of  $HNO_3$  is:

$$P_{HNO_3} = k_{NO_2}[NO_2][OH]_{SS} = \frac{P_r \times k_{NO_2}[NO_2]}{\sum k_i[A]_i + k_{NO_2}[NO_2]} \quad (3)$$

The total  $[HNO_3]$  is contributed by the chemical process ( $[HNO_3]_{chem}$ ) at a time frame of  $\Delta t$  and

35 transported from outside the domain boundaries ( $[HNO_3]_{trans}$ ) as follows:

$$[HNO_3] = [HNO_3]_{chem} + [HNO_3]_{trans} = \frac{P_r \times k_{NO_2}[NO_2]\Delta t}{\sum k_i[A]_i + k_{NO_2}[NO_2]} + [HNO_3]_{trans} \quad (4)$$

As-When  $[NO_2]$  is sufficiently ~~low-enough~~,  $[HNO_3]_{trans}$  ~~would~~ becomes comparable with  $[HNO_3]_{chem}$  to affect the total  $[HNO_3]$ . With the simple a ~~assumption of~~ assumption of  $[NO_2]$  is proportional to the emission

40 ~~reduction ratio~~ ratio ( $Er$ ), i.e., we have  $[NO_2] = [NO_2]_{control\_run} \times Er$ , ~~where  $Er$  is the emission ratio~~. With the assumptions of  $P_r \times \Delta t = 3$  and  $\sum k_i[A]_i : k_{NO_2}[NO_2]_{control\_run} = 7 : 5$ , ~~(the assumed variable values are applied to evaluate~~ the influence of transport term on the sensitivity,  $S_{NO_x,NO_3}$  can be evaluated.

Figure S141 shows  $HNO_3$  concentration and  $S_{NO_x,NO_3}$  ~~in this~~ under conditions with  $[HNO_3]_{trans} = 0, 0.2,$  and  $0.53$ , ~~which~~ representings no transported  $HNO_3$ , transported  $HNO_3$  equal to  $[HNO_3]_{chem}$  at  $NO_2 =$

45  $0.1$  and at  $NO_2 = 0.3$ , respectively.  $HNO_3$  increases as  $Er$  increases, but the increase gradually slows down. The v ~~Variations~~ in transported  $HNO_3$  ~~does~~ not alter the overall pattern of total  $HNO_3$ ; ~~it only~~ but do introduces differences in values (Fig. S144a). However, the trend of  $S_{NO_x,NO_3}$  is different (Fig. S144b).

~~In the absence of~~Without transported  $\text{HNO}_3$ ,  $S_{\text{NO}_x, \text{NO}_3}$  increases as  $Er$  decreases. Conversely, when  $[\text{HNO}_3]_{\text{trans}}$  is greater than 0,  $S_{\text{NO}_x, \text{NO}_3}$  ~~has~~ shows a transition point, occurring at  $Er$ , corresponding to a  $[\text{HNO}_3]_{\text{chem}}$  similar to  $[\text{HNO}_3]_{\text{trans}}$ . The scatter plot of  $S_{\text{NO}_x, \text{NO}_3}$  ~~is~~ calculated ~~based on~~ from the six discrete points with an interval of 0.2 to mimic the CMAQ simulation, ~~and~~ shows a similar trend under the influence of non-zero  $[\text{HNO}_3]_{\text{trans}}$ .

**Table S1: WRF-CMAQ model setting.**

	<b>Parameters</b>	<b>Setting</b>
<b>WRF</b> <b>v3.7.1</b>	Microphysics	WSM 5-class scheme
	Cumulus Parameterization	Kain-Fritsch
	Planetary Boundary Layer	YSU scheme
	Surface Layer	MM5 Monin-Obukhov scheme
	Land Surface	Unified Noah land-surface model
	Urban Surface	No
	Longwave Radiation	cam scheme
	Shortwave Radiation	cam scheme
	SST_update	Yes
<b>CMAQ</b> <b>v5.2.1</b>	Chemical mechanism	Cb06
	Horizontal advection	Yamo
	Vertical advection	WRF input
	Horizontal mixing/diffusion	Multiscale
	Aerosol	Aero 6
	Cloud option	ACM AE6
	Emission	TEDS 9.0

**Table S2: WRF-CMAQ resolution.**

		<b>D01</b>	<b>D02</b>	<b>D03</b>	<b>D04</b>
<b>WRF</b>	<b>Vertical Layer</b>	45	45	45	45
	<b>Grid size</b>	91×91	166×169	223×223	223×223
	<b>FDDA</b>	Yes	Yes	Yes	No
<b>CMAQ</b>	<b>Resolution</b>	81km	27km	9km	3km
	<b>Vertical Layer</b>	6	15	15	15
	<b>Grid size</b>	70×80	70×80	70×80	90×135

**Table S3: Box model initial conditions.**

parameter	value	Description*
<b>Temperature</b>	291 K	
<b>Cloud water</b>	0.376 g kg <sup>-1</sup>	
<b>CO<sub>2(g)</sub></b>	400 ppmv	Constant
<b>SO<sub>2(g)</sub></b>	7.13 ppbv	<sup>b</sup> SO <sub>2(g)</sub> + <sup>c</sup> dH <sub>2</sub> O <sub>2</sub>
<b><sup>a</sup>H<sub>2</sub>O<sub>2(g)</sub></b>	0.43 ppbv	
<b><sup>b</sup>O<sub>3(g)</sub></b>	18.7 ppbv	
<b>Total <sup>a</sup>NH<sub>3</sub></b>	73.4 ppbv × <sup>d</sup> Er	NH <sub>3(g)</sub> + NH <sub>4</sub> <sup>+</sup> (I+J+K)
<b>Total <sup>a</sup>HNO<sub>3</sub></b>	12.3 ppbv	HNO <sub>3(g)</sub> + NO <sub>3</sub> <sup>-</sup> (I+J+K)
<b>SO<sub>4</sub><sup>2-</sup></b>	0.088 μg m <sup>-3</sup>	<sup>b</sup> SO <sub>4</sub> <sup>2-</sup> (I+J+K) – <sup>c</sup> dH <sub>2</sub> O <sub>2</sub>
<b><sup>a</sup>Fe<sup>3+</sup></b>	0.0238 μg m <sup>-3</sup>	Fe(III) available for sulfate oxidation
<b><sup>a</sup>Mn<sup>2+</sup></b>	0.035 μg m <sup>-3</sup>	Mn(II) available for sulfate oxidation
<b><sup>a</sup>Na<sup>+</sup></b>	0.48	I+J+K
<b><sup>a</sup>K<sup>+</sup></b>	0.82	J+K
<b><sup>a</sup>Ca<sup>2+</sup></b>	1.38	J+K
<b><sup>a</sup>Mg<sup>2+</sup></b>	1.00	J+K
<b><sup>a</sup>Cl<sup>-</sup></b>	0.64	I+J+K

\* I, J, K denotes Aitken, accumulation, and coarse modes in particle phase from CMAQ output.

60 \* Condition: a grid point along the coast of Taichung (24.203° N, 120.5053° E, the second layer, ~ 68.5 m a.s.l) at 8:00 am local time on 3<sup>rd</sup> December 2018 from CMAQ.

<sup>a</sup> The concentration from the control run.

<sup>b</sup> The concentration from the NH3\_02x run (NH<sub>3</sub> emission reduced to 0.2x of control run).

<sup>c</sup> dH<sub>2</sub>O<sub>2</sub> is the H<sub>2</sub>O<sub>2</sub> difference concentration (control run – NH3-02x run).

65 <sup>d</sup> Er ranges from 0.2 to 1.0 at 0.1 intervals

**Table S4: Reactions and rate constants used in the box model (from Seinfeld and Pandis (2006))**

<b>Dissolution reaction</b>		<b>Henry's constant (M atm<sup>-1</sup>)</b>
1.	$\text{CO}_2 + \text{H}_2\text{O} \leftrightarrow \text{CO}_2 \cdot \text{H}_2\text{O}$	$H_{\text{CO}_2} = 0.034$
2.	$\text{SO}_2 + \text{H}_2\text{O} \leftrightarrow \text{SO}_2 \cdot \text{H}_2\text{O}$	$H_{\text{SO}_2} = 1.23$
3.	$\text{HNO}_3(\text{g}) \leftrightarrow \text{HNO}_3(\text{aq})$	$H_{\text{HNO}_3} = 2.1 \times 10^5$
4.	$\text{NH}_3 + \text{H}_2\text{O} \leftrightarrow \text{NH}_3 \cdot \text{H}_2\text{O}$	$H_{\text{NH}_3} = 62$
5.	$\text{O}_3(\text{g}) \leftrightarrow \text{O}_3(\text{aq})$	$H_{\text{O}_3} = 1.14 \times 10^{-2}$
6.	$\text{H}_2\text{O}_2(\text{g}) \leftrightarrow \text{H}_2\text{O}_2(\text{aq})$	$H_{\text{H}_2\text{O}_2} = 1 \times 10^5$
<b>Dissociation reaction</b>		<b>Rate constant (M)</b>
7.	$\text{CO}_2 \cdot \text{H}_2\text{O} \leftrightarrow \text{HCO}_3^- + \text{H}^+$ $\text{HCO}_3^- \leftrightarrow \text{CO}_3^{2-} + \text{H}^+$	$k_{c1} = 4.2 \times 10^{-7}$ $k_{c2} = 5.61 \times 10^{-11}$
8.	$\text{SO}_2 \cdot \text{H}_2\text{O} \leftrightarrow \text{HSO}_3^- + \text{H}^+$ $\text{HSO}_3^- \leftrightarrow \text{SO}_3^{2-} + \text{H}^+$	$k_{s1} = 1.3 \times 10^{-2}$ $k_{s2} = 6.6 \times 10^{-8}$
9.	$\text{HNO}_3(\text{aq}) \leftrightarrow \text{NO}_3^- + \text{H}^+$	$k_{a1} = 15.4$
10.	$\text{NH}_3 \cdot \text{H}_2\text{O} \leftrightarrow \text{NH}_4^+ + \text{OH}^-$	$k_{a1} = 1.7 \times 10^{-5}$
11.	$\text{H}_2\text{SO}_4 \leftrightarrow \text{HSO}_4^- + \text{H}^+$ $\text{HSO}_4^- \leftrightarrow \text{SO}_4^{2-} + \text{H}^+$	as a complete dissociation $k_{a2} = 1.2 \times 10^{-2}$
12.	$\text{H}_2\text{O} \leftrightarrow \text{H}^+ + \text{OH}^-$	
<b>Aqueous oxidation reaction</b>		<b>Rate constant (M<sup>-1</sup>s<sup>-1</sup>)</b>
13.	$\text{SO}_2 + \text{O}_3 + \text{H}_2\text{O} \rightarrow \text{SO}_4^{2-} + \text{O}_2 + 2\text{H}^+$ $\text{HSO}_3^- + \text{O}_3 \rightarrow \text{SO}_4^{2-} + \text{O}_2 + \text{H}^+$ $\text{SO}_3^{2-} + \text{O}_3 \rightarrow \text{SO}_4^{2-} + \text{O}_2$	$k_{\text{O}_3,1} = 2.4 \times 10^4$ $k_{\text{O}_3,2} = 3.7 \times 10^5$ $k_{\text{O}_3,2} = 1.5 \times 10^9$
14.	$\text{HSO}_3^- + \text{H}_2\text{O}_2 + \text{H}^+ \rightarrow \text{SO}_4^{2-} + 2\text{H}^+ + \text{H}_2\text{O}$	$k_{\text{H}_2\text{O}_2} = 7.45 \times 10^7$
15.	$\text{S(IV)} + \frac{1}{2} \text{O}_2 \xrightarrow{\text{Mn}^{2+}, \text{Fe}^{3+}} \text{S(VI)}$	$k_{\text{Mn}} = 750; k_{\text{Fe}} = 2600;$ $k_{\text{Mn,Fe}} = 1.0 \times 10^{10}$

**Table S5: Statistics of air temperature, relative humidity, CO, and O<sub>3</sub> of MOENV observation and model simulation results.**

	Tamsui	Shalu	Taixi	Qianzhen
<b>Temperature (degree C)</b>				
Mean value of MOENV	18.61	20.19	20.00	23.31
Mean value of WRF	18.48	19.50	19.05	22.39
Correlation coefficient	0.87	0.93	0.84	0.93
Mean bias error	-0.18	-0.69	-0.95	-0.92
Mean absolute error	1.33	1.10	1.47	1.34
<b>RH (%)</b>				
Mean value of MOENV	85.12	74.97	82.85	69.49
Mean value of WRF	80.42	76.49	80.71	69.95
Correlation coefficient	0.71	0.84	0.58	0.86
Mean bias error	-4.23	1.52	-2.14	0.46
Mean absolute error	7.31	6.23	6.75	4.78
<b>CO (ppbv)</b>				
Mean value of MOENV	331.98	355.42	258.98	644.20
Mean value of CMAQ	137.84	143.09	129.03	266.13
Correlation coefficient	0.59	0.53	0.46	0.62
Mean bias error	-194.05	-212.32	-129.94	-377.72
Mean absolute error	196.13	212.32	130.95	378.77
<b>O<sub>3</sub> (ppbv)</b>				
Mean value of MOENV	35.05	31.43	37.74	26.77
Mean value of CMAQ	47.13	42.73	42.57	32.51
Correlation coefficient	0.66	0.73	0.58	0.84
Mean bias error	12.07	11.29	4.67	5.76
Mean absolute error	13.0	12.93	8.94	11.05

$$\text{Correlation coefficient} = \frac{\sum_{i=1}^n (m_i - \bar{m})(o_i - \bar{o})}{\sqrt{\sum_{i=1}^n (m_i - \bar{m})^2} \sqrt{\sum_{i=1}^n (o_i - \bar{o})^2}}$$

$$\text{Mean bias error} = \overline{(m_i - o_i)}; \text{Mean absolute error} = \overline{|(m_i - o_i)|}$$

75 where  $m_i$  and  $o_i$  are the wind speed or concentrations of model and observation at time  $i$ , respectively, and  $\bar{m}$  and  $\bar{o}$  are their average over December 2018.



**Table S6: Mean contribution of sulfate formation in each air pollution zone (elevation altitude below 200\_m a.s.l.).**

	<b>Gas phase processes</b>	<b>Aqueous phase processes</b>	<b>Other processes</b>
northern Taiwan	8.4-%	21.5-%	70.1-%
Chu-Miao area	11.2-%	28.5-%	60.3-%
central Taiwan	13.2-%	30.5-%	56.3-%
Yun-Chia-Nan area	16.5-%	27.6-%	55.9-%
Kao-Ping area	19.8-%	23.7-%	56.6-%

80

**Table S7: Statistics of the sensitivity of emission reductions on PM<sub>2.5</sub> concentration sensitivity coefficient of NO<sub>x</sub> ( $S_{NO_x, PM_{2.5}}$ ) and NH<sub>3</sub> ( $S_{NH_3, PM_{2.5}}$ ) in each air pollution zone (elevation altitude below 200\_m a.s.l.) under the current conditions (at NO<sub>x</sub> emission ratio of 0.9).**

	$S_{NO_x, PM_{2.5}}$			$S_{NH_3, PM_{2.5}}$		
	Mean	Q1	Q3	Mean	Q1	Q3
Northern Taiwan	0.15	0.12	0.19	0.12	0.11	0.14
Chu-Miao area	0.20	0.18	0.22	0.17	0.16	0.19
Central Taiwan	0.23	0.20	0.25	0.19	0.18	0.21
Yun-Chia-Nan area	0.33	0.30	0.36	0.19	0.18	0.20
Kao-Ping area	0.34	0.31	0.41	0.19	0.17	0.21

Mean: Arithmetic-arithmetic mean; Q1: 25th percentile; Q3: 75th percentile.

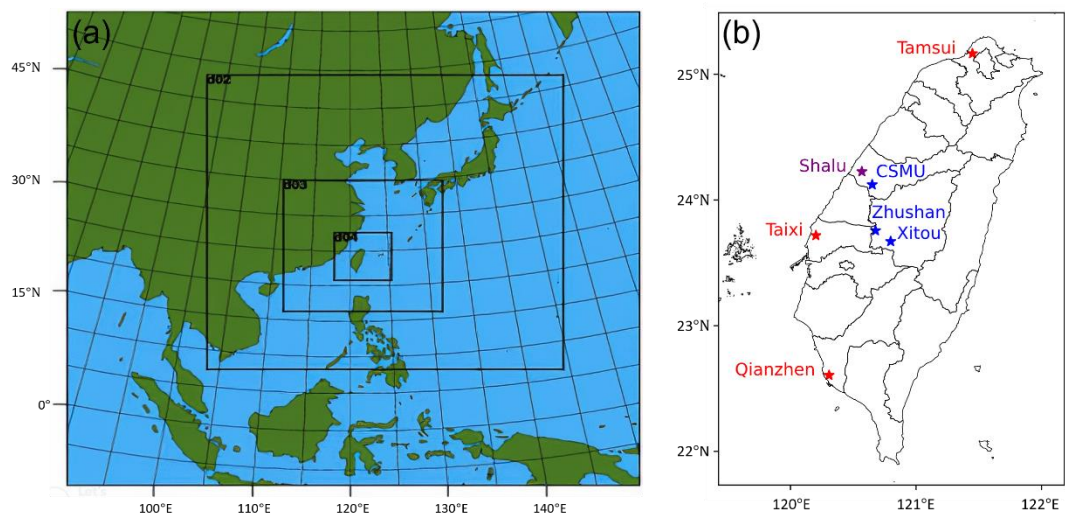
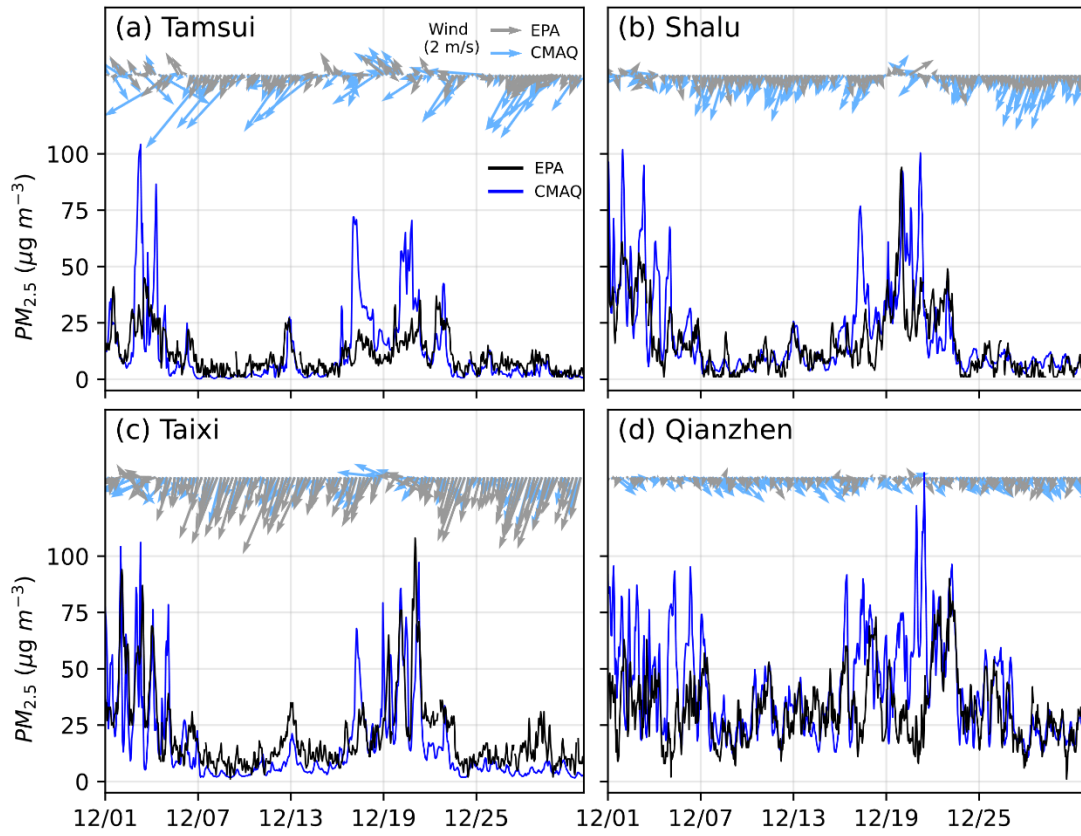
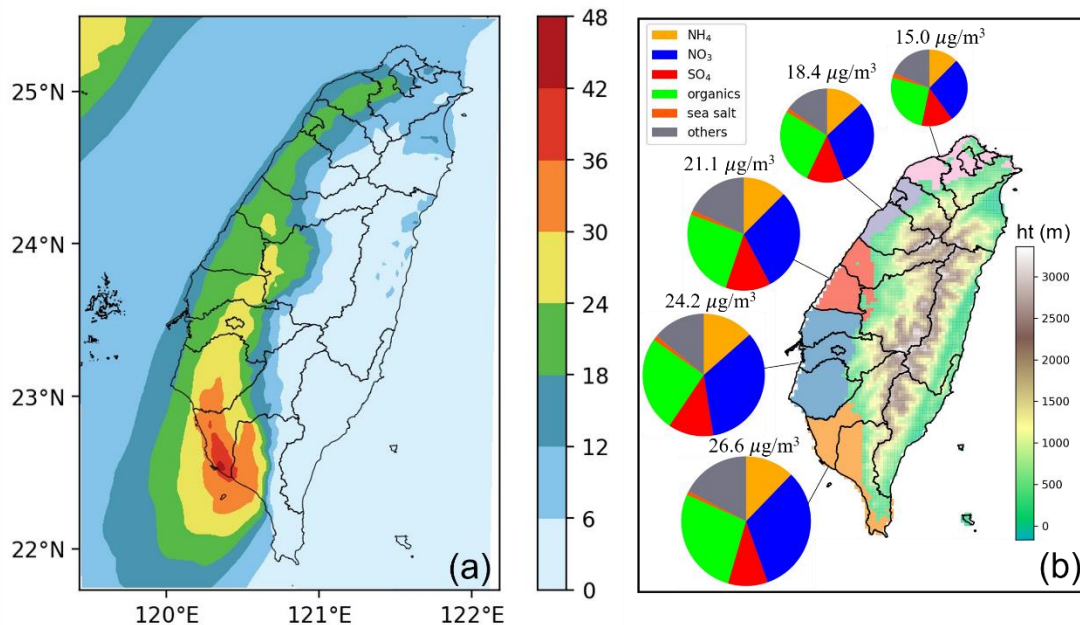


**Figure S1: (a) WPS domain configuration. (b) CMAQ d04 domain. Red points (★) are MOENV stations, blue points (★) are indicate PM components measurement stations, and purple point (★) is Shalu station, having both MOENV EPA data and PM components data.**

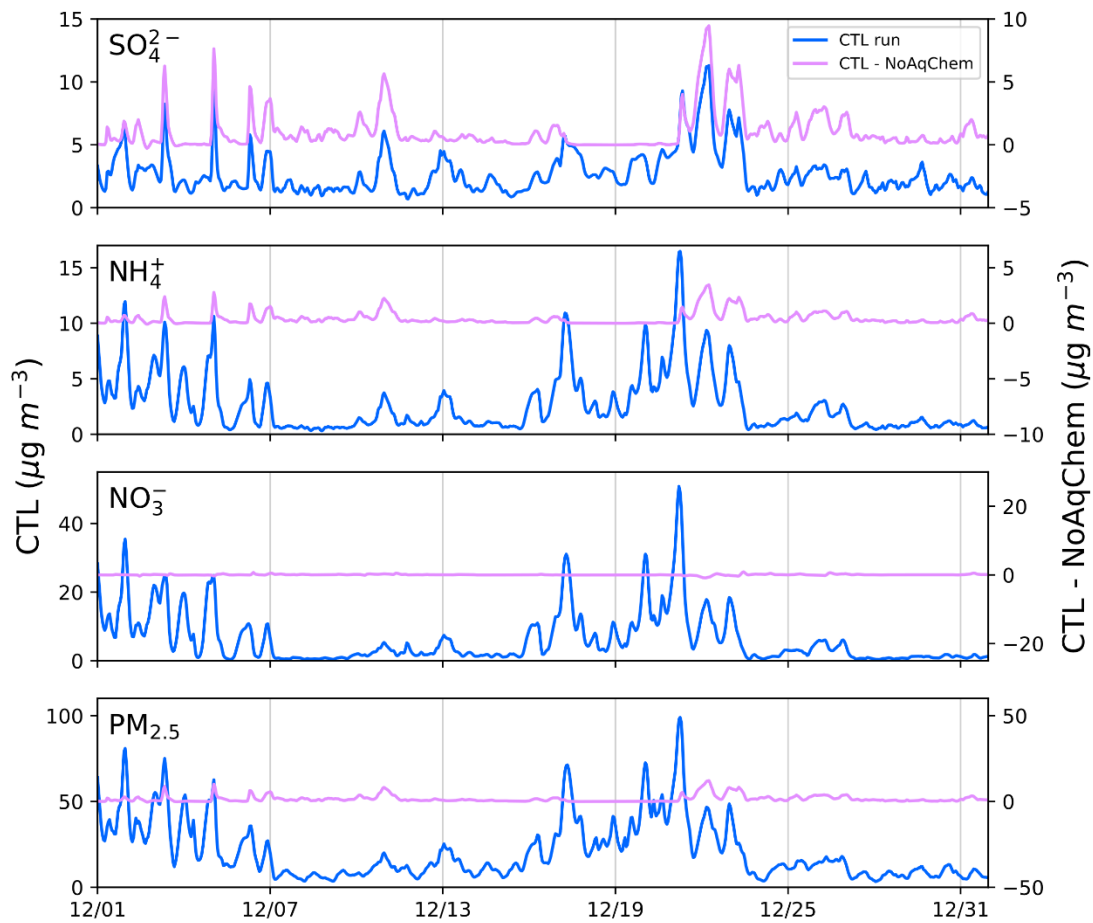


90

Figure S2: The comparison of wind field and  $PM_{2.5}$  between MOENV ground observations and CMAQ surface layer data.

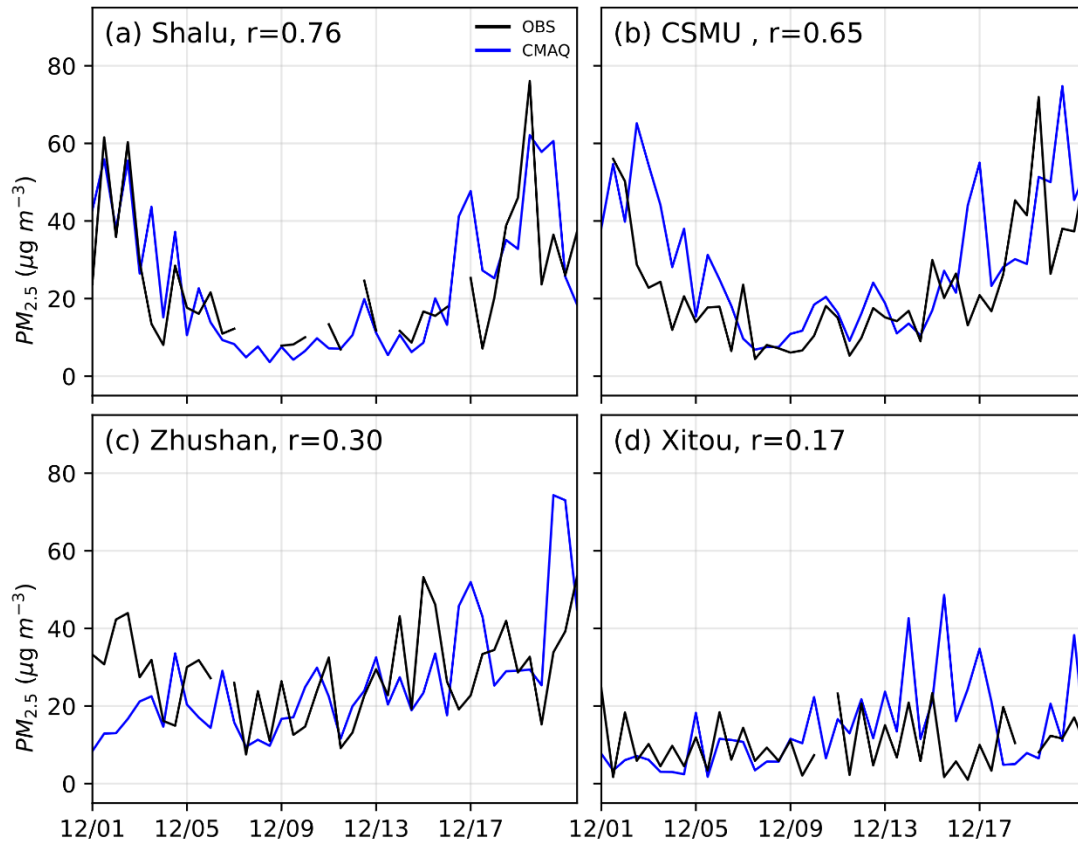


95 Figure S3: Model results for (a) Average PM<sub>2.5</sub> concentration ( $\mu\text{g m}^{-3}$ ). (b) The composition fraction and PM<sub>2.5</sub> concentrations for different regions (different shading colors) at-for elevation less than 200 m altitude above sea level. (From north to south, the regions from north to south are northern Taiwan (pink), Chu-Miao (purple), central Taiwan (red), Yun-Chia-Nan (blue), and Kao-Ping (orange)). The components are-is shown in legend. The color bar is the height above sea level. Conditions: average data from 1-31for December 2018 for-at the surface layer.



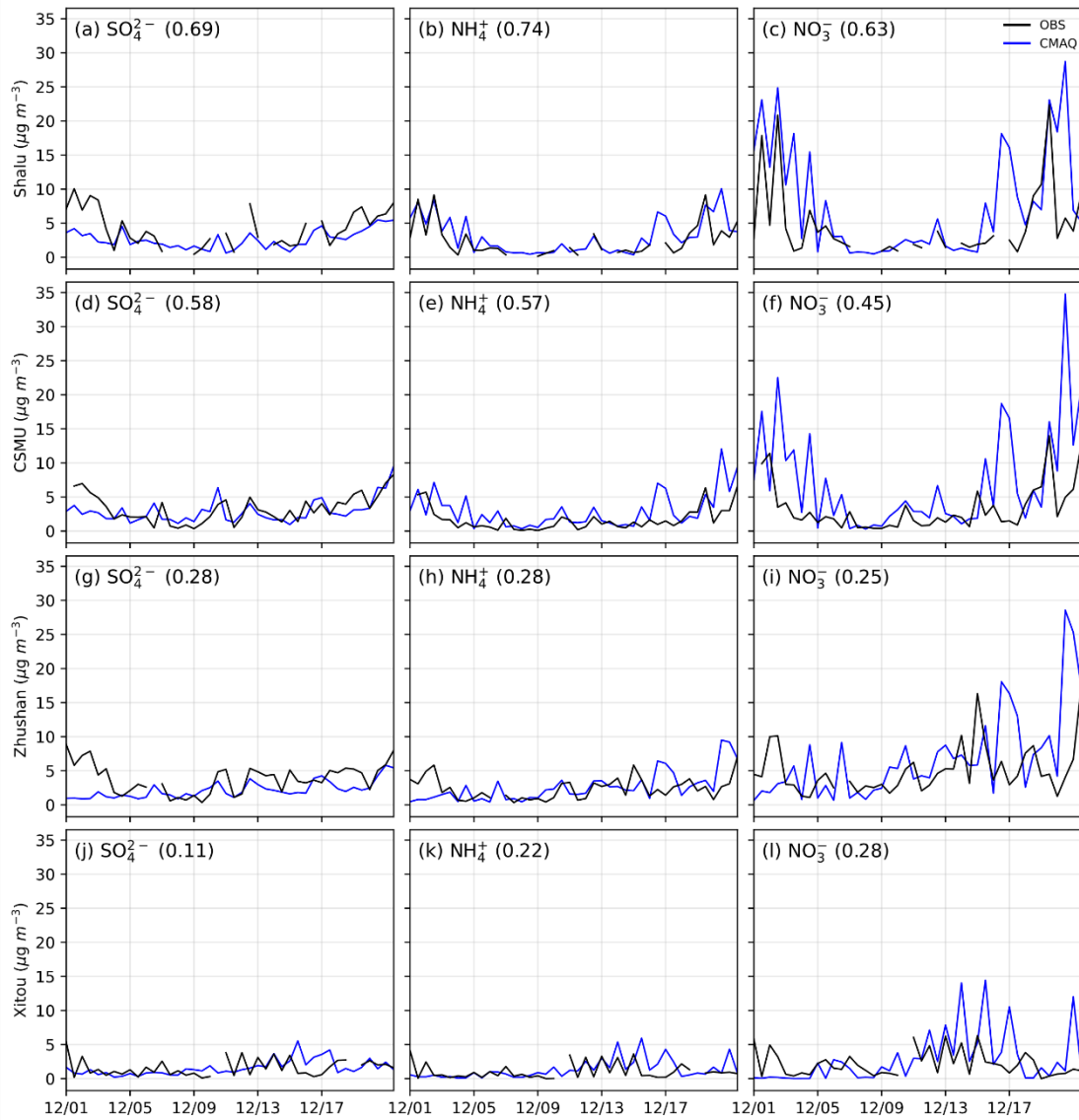
100

Figure S4: Sulfate, ammonium, nitrate, and  $\text{PM}_{2.5}$  concentrations of control run (blue line, left y-axis) and the difference between control and NoAqChem runs (pink line, right y-axis). The left and right y-axes have the same scale but different ranges. Conditions: average data for central Taiwan for at the surface layer.



105

**Figure S5: The comparison of PM<sub>2.5</sub> between observation and CMAQ surface layer data in central Taiwan (r: correlation coefficient).**



110 **Figure S6: The comparison of sulfate, ammonium, and nitrate between observation and CMAQ surface layer data in central Taiwan; (the correlation coefficients are indicated in parentheses).**



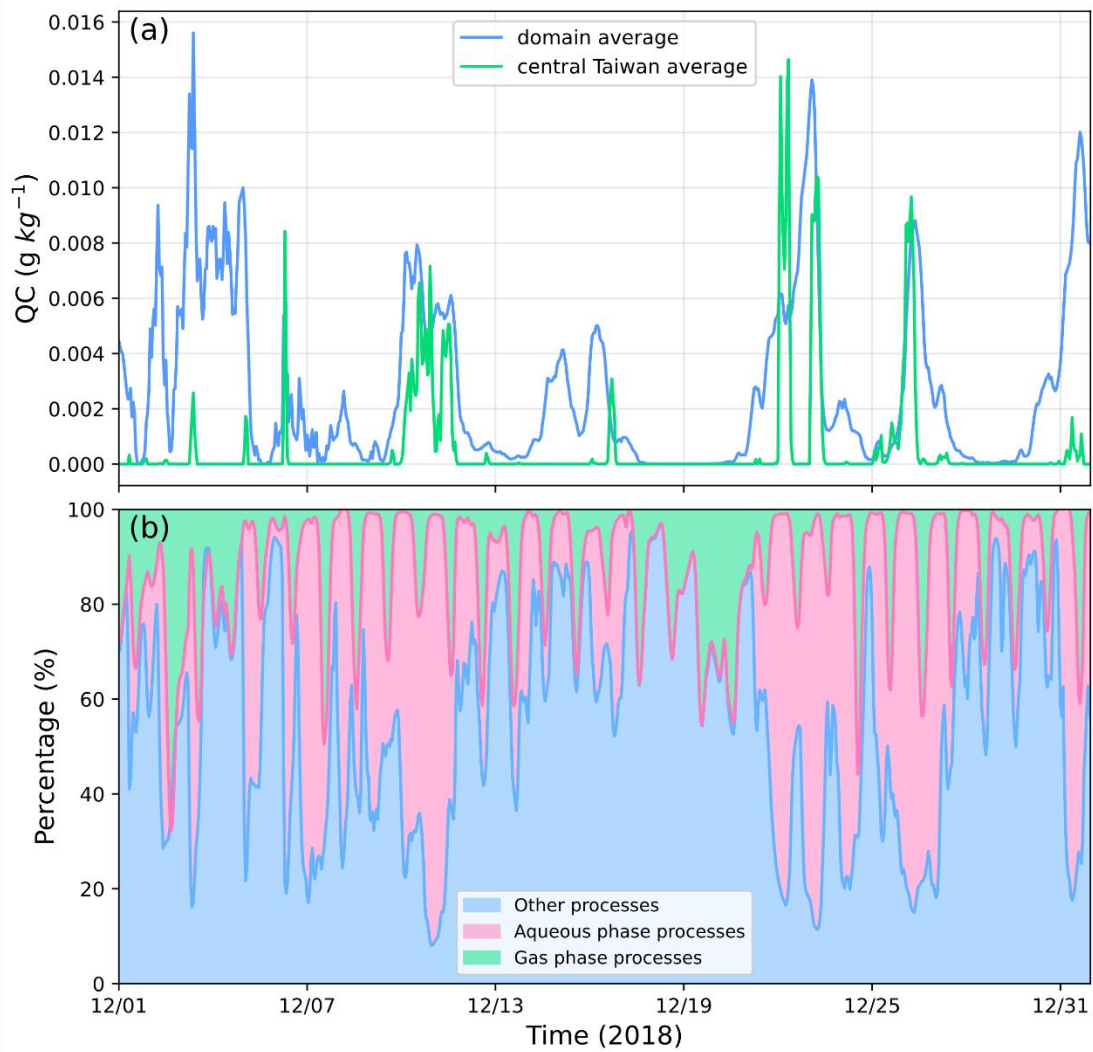
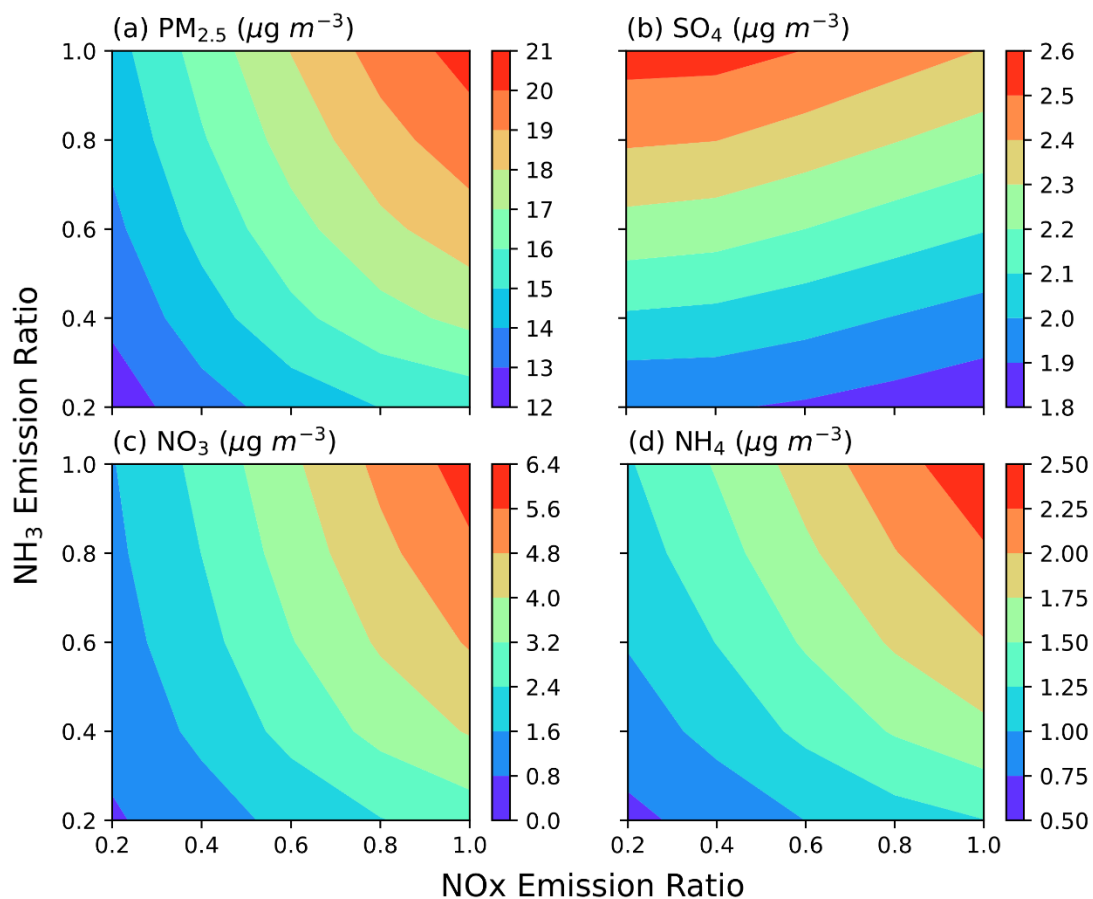
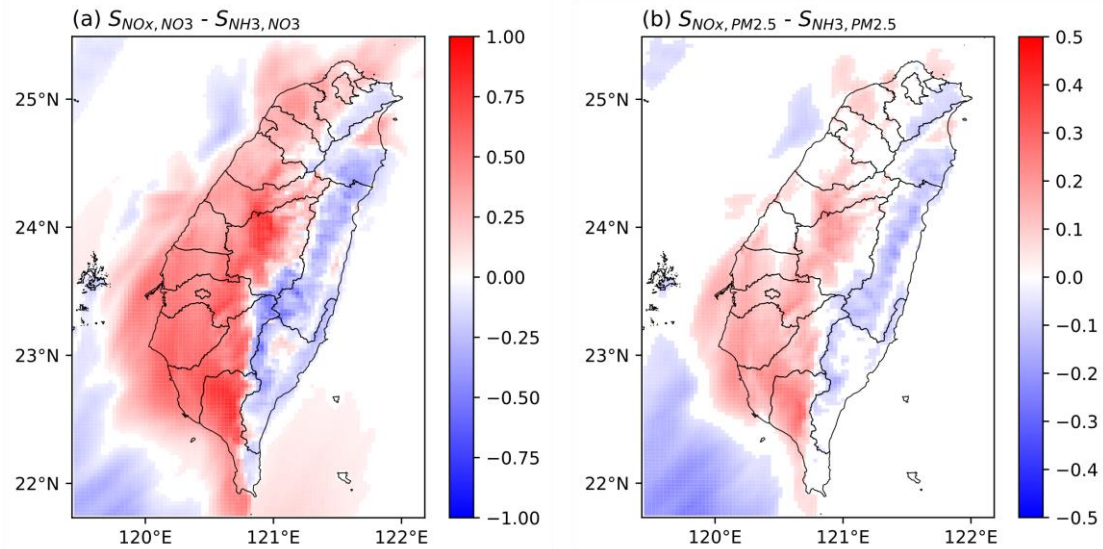


Figure S67: (a) Average cloud water content within the planetary boundary layers. (b) Surface layer average sulfate source contributions in central Taiwan.

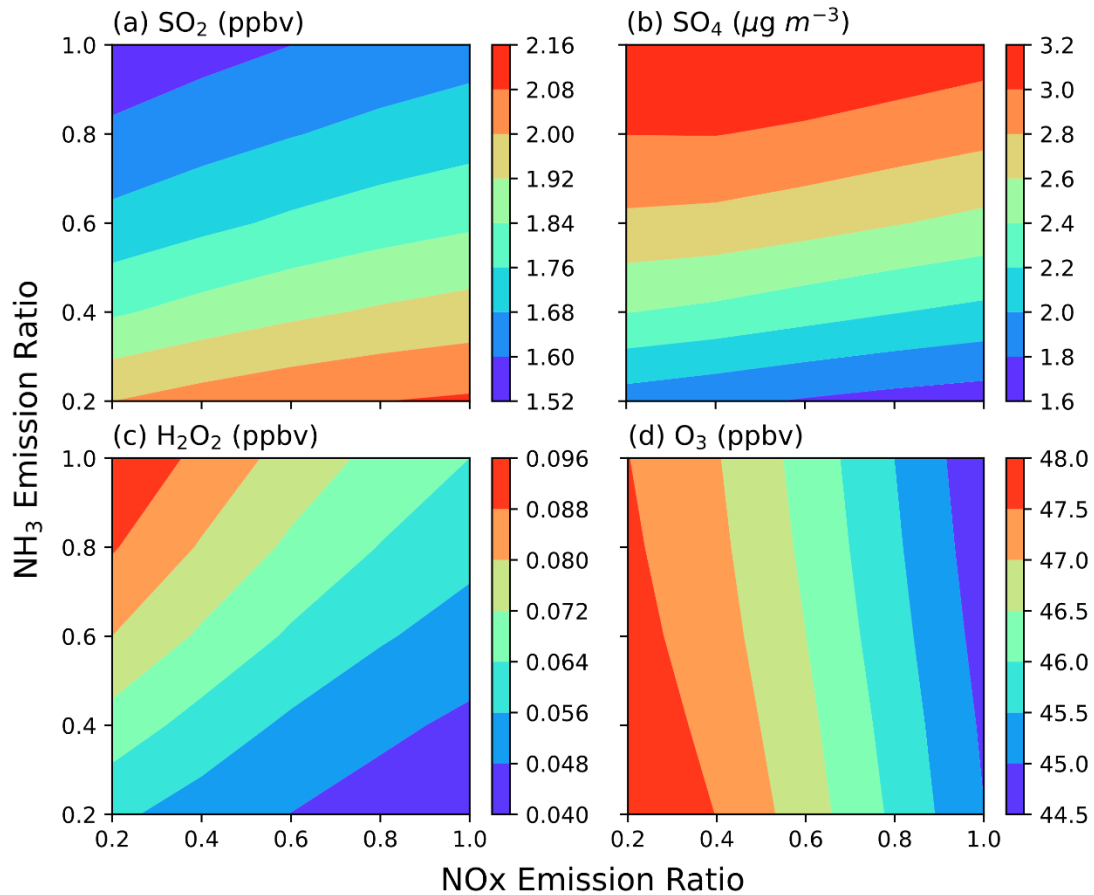


115

Figure S87: (a)  $\text{PM}_{2.5}$ , (b) sulfate, (c) nitrate, and (d) ammonium average concentrations as a function of NOx (x-axis) and NH<sub>3</sub> (y-axis) emission ratios. Conditions: average data of central Taiwan from 1<sup>st</sup> to 14<sup>th</sup> December 2018 for at the surface layer.

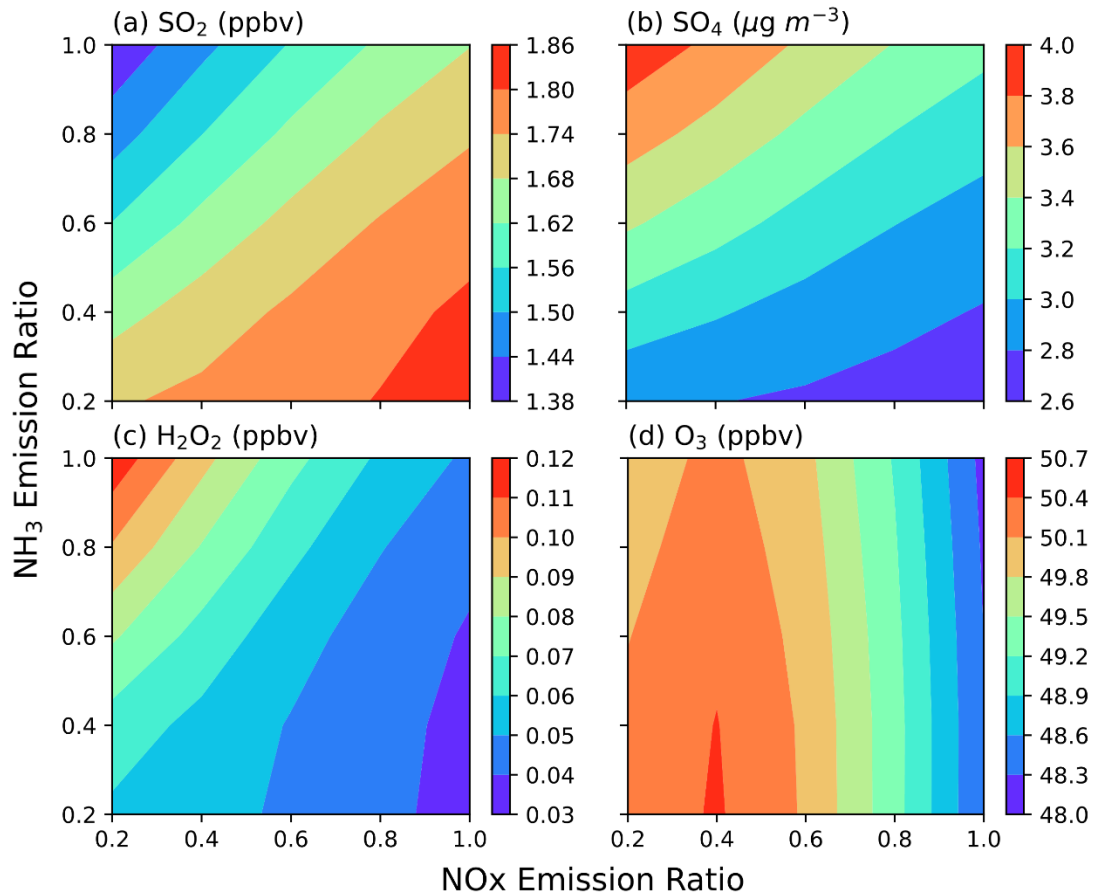


120 **Figure S89:** The difference in sensitivity map of (a) nitrate and (b)  $PM_{2.5}$  sensitivity coefficient map between  $NO_x$  and  $NH_3$  under the current condition (at  $NO_x$  emission ratio of 0.9). Red regimes areas (positive) represent  $NO_x$ -sensitive, blue regimes areas (negative) represent  $NH_3$ -sensitive, and white regimes areas represent neutral with values between -0.05 and 0.05. Conditions: average data ~~from~~ for 1-31 December 2018 ~~for~~ at the surface layer.



125

**Figure S910:** Average in-cloud concentrations of (a)  $\text{SO}_2$ , (b) sulfate, (c)  $\text{H}_2\text{O}_2$ , and (d) ~~ozone~~  $\text{O}_3$  concentration as a function of  $\text{NO}_x$  (x-axis) and  $\text{NH}_3$  (y-axis) emission ratios. Conditions: average data ~~of for the cloud grid points of~~ western Taiwan land regions in domain 4 from 1<sup>st</sup> to 14<sup>th</sup> December 2018 ~~for the cloud grid points~~.



130

**Figure S110:** Average in-cloud concentrations of (a) SO<sub>2</sub>, (b) sulfate, (c) H<sub>2</sub>O<sub>2</sub>, and (d) ozone concentration as a function of NOx (x-axis) and NH<sub>3</sub> (y-axis) emission ratios. Conditions: average data for the cloud grid points of sea regions, west of 121°E in domain 4, from 1<sup>st</sup> to -14<sup>th</sup> December 2018 for the cloud grid points.

135

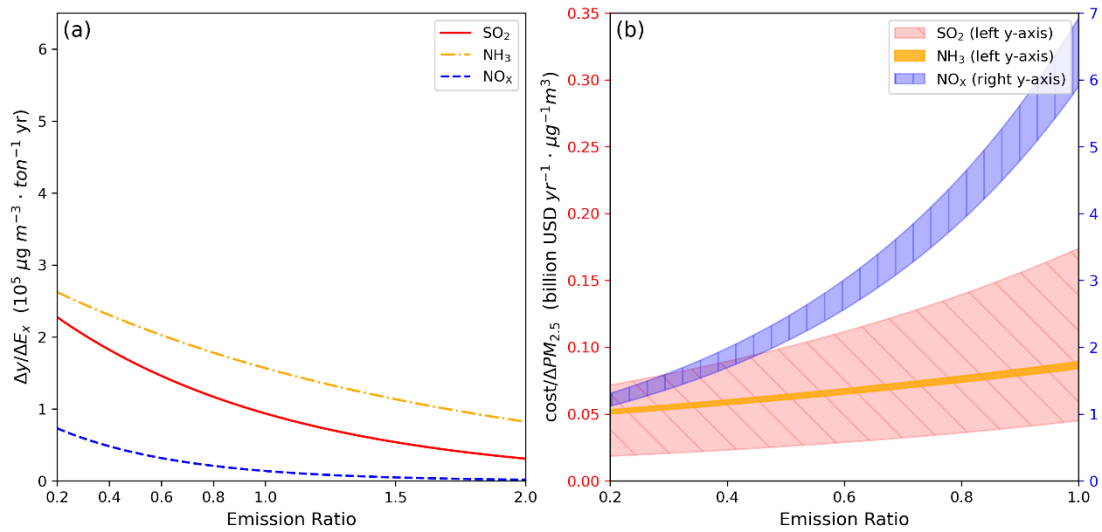
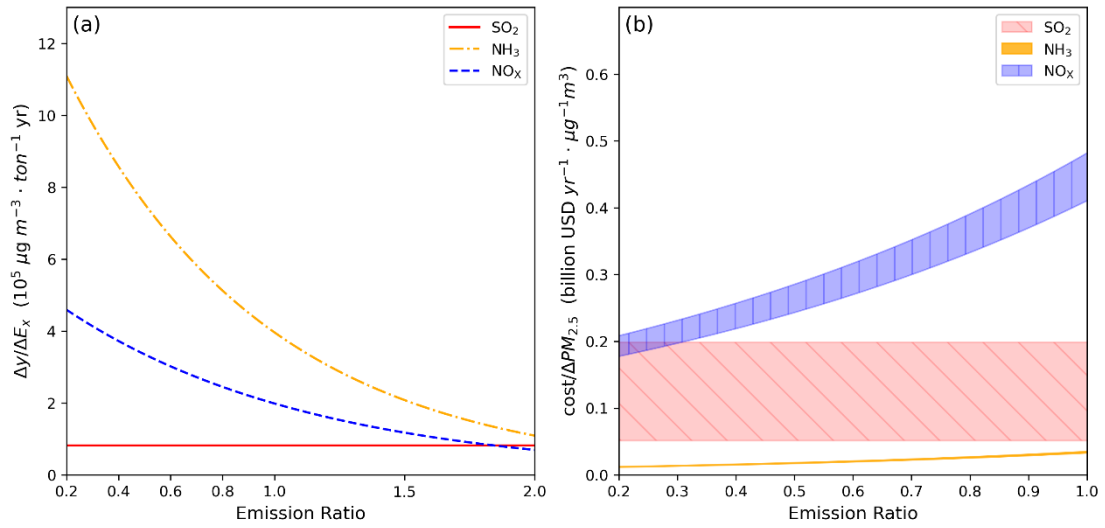


**Figure S12: (a) PM<sub>2.5</sub> reduction efficiency and (b) reduction cost as a function of emission ratio for SO<sub>2</sub>, NH<sub>3</sub>, and NO<sub>x</sub> during the clean period from 6<sup>th</sup>-12<sup>th</sup> December 2018.**



140

**Figure S13: (a) PM<sub>2.5</sub> reduction efficiency and (b) reduction cost as a function of emission ratio for SO<sub>2</sub>, NH<sub>3</sub>, and NO<sub>x</sub> during the high pollution period from 16<sup>th</sup>-22<sup>th</sup> December 2018.**

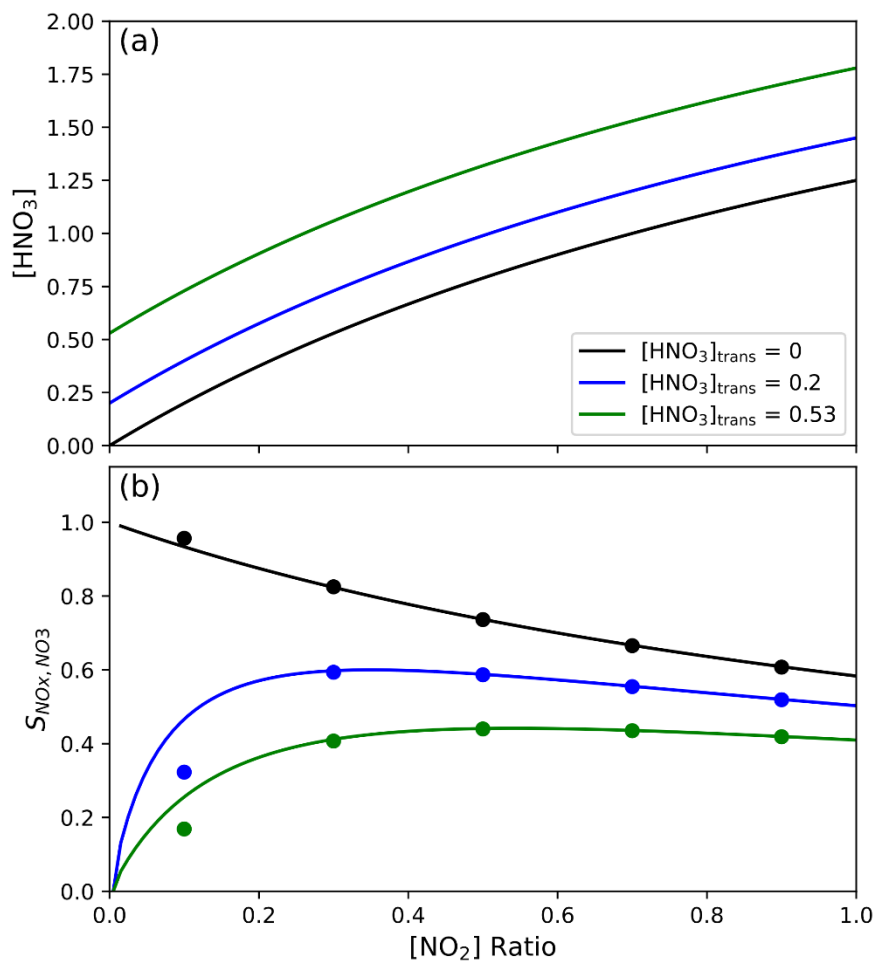


Figure S141: (a) HNO<sub>3</sub> concentration and (b) nitrate sensitivity coefficient of NO<sub>x</sub> ( $S_{NO_x, NO_3}$ ) as a function of NO<sub>2</sub> emission ratio for three conditions of [HNO<sub>3</sub>]<sub>trans</sub> = 0, 0.2, and 0.53.



**Reference**

Seinfeld, J. H., and Pandis, S. N.: Atmospheric Chemistry and Physics: From Air Pollution to Climate Change, Wiley, 2006.